Effective Hamiltonian for electron waves in artificial graphene: A first-principles derivation

Sylvain Lannebère and Mário G. Silveirinha

University of Coimbra, Department of Electrical Engineering – Instituto de Telecomunicações, Coimbra 3030-290, Portugal

We propose a first-principles effective medium formalism to study the propagation of electron waves in semiconductor heterostructures with a zero band gap. Our theory confirms that near the K point the dynamics of a two-dimensional electron gas modulated by an external electrostatic potential with honeycomb symmetry is described by the same pseudospinor formalism and Dirac massless equation as a graphene monolayer. Furthermore, we highlight that even though other superlattices based on semiconductors with a zincblende-type structure can have a zero band-gap and a linear energy-momentum dispersion, the corresponding effective medium Hamiltonian is rather different from that of graphene, and can be based on a single-component wave function.

PACS number(s): 73.21.Cd, 73.23.−b, 73.22.−f

I. INTRODUCTION

The experimental discovery of graphene in 2004 [1] opened the door to a large scientific activity, and nowadays graphene physics is one of the most vibrant research fields in condensed matter physics. One of the fascinating electronic properties of graphene is that low-energy electrons may be described by a 2D massless Dirac equation. Consequently, the electron states have a linear energy dispersion with a zero band gap [2,3]. This feature is interesting not only because it may enable ultrafast carbon-based electronics due to the high electron mobility, but also to create tunable "one-atom-thick" platforms for infrared photonic functions [4–7] with a strong non linear optical response [8].

Recently, other mechanisms have been suggested to mimic the extraordinary properties of graphene, such as using ultracold atoms in hexagonal or honeycomb optical lattices [9–12], using photonic crystals ("photonic graphene") [13], or applying a periodic potential onto a two-dimensional electron gas (2DEG) [14,15]. This latter idea was first described in Ref. [16], where the authors studied a nanopatterned electron gas with hexagonal symmetry, and demonstrated that the electrons behavior is governed by a massless Dirac equation. The case of a potential with honeycomb symmetry was considered in Ref. [17], which also reported a possible realization based on modulation-doped GaAs quantum wells.

The conclusion that electrons may behave as massless Dirac fermions in a 2DEG modulated by an external potential is largely rooted in the observation that the energy dispersion is linear near the corners of the Brillouin zone and on an analogy with graphene [16,17]. In our view, it would be desirable to have a more solid theoretical foundation of such an important result, and have a more complete understanding if linear dispersing bands do always imply that the time dynamics of the electron waves is described by a massless Dirac equation. Indeed, one may wonder if a different type of physics may be as well compatible with linear dispersing bands.

With this objective in mind, in this paper, we develop a first-principles effective medium approach to characterize a two-dimensional gas of noninteracting electrons modulated by an external potential. Our theory is based on the effective medium theory for electron waves developed in Ref. [18]. In that work, it was shown that it is possible to introduce an effective Hamiltonian that describes exactly the time evolution

of electron states that vary slowly on the scale of the unit cell. Furthermore, the electronic band structure obtained from the effective medium Hamiltonian is exactly coincident with what is found from the microscopic Hamiltonian [18]. Here, we apply an extended version of this theory to demonstrate from first principles that the electron wave-function envelope in a nanopatterned 2DEG with honeycomb symmetry satisfies, indeed, the 2D massless Dirac equation. Moreover, we also investigate the effective medium description of superlattices [19] based on semiconductors with zinc-blende-type structure. Consistent with our previous studies [20–22], it is found the electron energy dispersion may be linear for some structural parameters. Interestingly, it is shown that in this system, the electrons do not have a pseudospin degree of freedom, quite different from what happens in graphene wherein the electrons are chiral fermions.

This paper is organized as follows. In Sec. II, we present a brief overview of the theory of Ref. [18], and apply it to characterize a 2DEG modulated by an external electrostatic potential with honeycomb symmetry. It is shown that a direct application of the method yields a single-component Hamiltonian characterized by a strongly nonlocal (spatially dispersive) response. To circumvent this problem, in Sec. III, the effective medium approach is extended to allow for a pseudospinor formalism. It is proven that, similar to graphene, the electrons in the superlattice behave as Dirac fermions and are described by the massless Dirac equation. A parametric study of the influence of the external potential amplitude and of the geometry on the effective Hamiltonian is presented. In Sec. IV, we analyze an hexagonal superlattice formed by mercury-cadmium-telluride compounds, and prove that the time evolution of electron waves in this second platform can be done based on a single-component wave function. Finally, in Sec. V the conclusions are drawn.

II. SINGLE-COMPONENT HAMILTONIAN FOR A POTENTIAL WITH THE HONEYCOMB SYMMETRY

In this section, we describe how to obtain the single-component effective medium Hamiltonian for an artificial graphene platform based on a two-dimensional electron gas, and discuss the characteristics and limitations of such a description.

A. Overview of the effective medium approach

In the following, we present a brief overview of the effective medium approach developed in Ref. [18]. The use of effective medium concepts (e.g., the effective mass) has a long tradition in condensed matter physics, and some relevant works can be found in Refs. [23–28].

To begin with, we consider a periodic system (e.g., a semiconductor superlattice) described at the microscopic level by the Hamiltonian $\hat{H}$ and whose time evolution is determined by the Schrödinger equation

$$\hat{H}\psi(\mathbf{r},t) = i\hbar\frac{\partial}{\partial t}\psi(\mathbf{r},t). \tag{1}$$

The key idea of the method is to introduce an effective Hamiltonian $\hat{H}_{\text{ef}}$ that describes exactly the time evolution of initial ($t = 0$) "macroscopic" states, through a homogenized Schrödinger equation

$$(\hat{H}_{\text{ef}}\Psi)(\mathbf{r},t) = i\hbar\frac{\partial}{\partial t}\Psi(\mathbf{r},t). \tag{2}$$

We say that an electron state ψ is macroscopic if it is invariant after spatial averaging: $\psi(\mathbf{r}) = \{\psi(\mathbf{r})\}_{\text{av}}$, and we define $\Psi(\mathbf{r},t) = \{\psi(\mathbf{r},t)\}_{\text{av}}$. Here, we consider that the spatial averaging operator $\{\}_{\text{av}}$ is equivalent to an ideal band-pass spatial filter such that for a generic function g depending on the spatial variable $\mathbf{r}$

$$\{g(\mathbf{r})\}_{\text{av}} = \int g(\mathbf{r} - \mathbf{r}')w(\mathbf{r}')d^N\mathbf{r}', \tag{3}$$

where w is a test function whose Fourier transform $\tilde{w}(\mathbf{k}) = \int w(\mathbf{r})e^{-i\mathbf{k}\cdot\mathbf{r}}d^N\mathbf{r}$ has the following properties [18,29]:

$$\tilde{w}(\mathbf{k}) = \begin{cases} 1, & \mathbf{k} \in BZ \\ 0, & \mathbf{k} \notin BZ \end{cases}, \tag{4}$$

where $\mathbf{k}$ is the wave vector and BZ stands for a suitable primitive cell in the reciprocal space. For example, if the states that determine the physics of the system are near the Γ point then BZ should be taken as the first Brillouin zone. In the above, N represents the number of relevant spatial dimensions (in this paper $N = 2$). From a physical point of view, the property $\psi(\mathbf{r}) = \{\psi(\mathbf{r})\}_{\text{av}}$ is equivalent to say that the electron state cannot be more localized than the characteristic spatial period of the system. The effective Hamiltonian $\hat{H}_{\text{ef}}$ is defined so that if $\psi_{t=0}(\mathbf{r}) = \{\psi_{t=0}(\mathbf{r})\}_{\text{av}}$, i.e., if the initial time state is macroscopic, then the solutions of Eqs. (1) and (2) with the same initial time conditions are linked by $\Psi(\mathbf{r},t) = \{\psi(\mathbf{r},t)\}_{\text{av}}$. In other words, the effective Hamiltonian describes the dynamics of the smooth part of the wave function $\psi(\mathbf{r},t)$. A consequence of this property is that for an initial macroscopic state:

$$(\hat{H}_{\text{ef}}\Psi)(\mathbf{r},t) = \{(\hat{H}\psi)(\mathbf{r},t)\}_{\text{av}}, \quad t > 0. \tag{5}$$

Calculating the unilateral Laplace transform of both sides of the equation [e.g.. the Laplace transform of $\psi(\mathbf{r},t)$ is $\psi(\mathbf{r},\omega) = \int_0^\infty dt\,\psi(\mathbf{r},t)\,e^{i\omega t}$], we get

$$(\hat{H}_{\text{ef}}\Psi)(\mathbf{r},\omega) = \{(\hat{H}\psi)(\mathbf{r},\omega)\}_{\text{av}}. \tag{6}$$

The above identity may be used to numerically determine the effective Hamiltonian as detailed below.

It was shown in Ref. [18] that the action of the operator $\hat{H}_{\text{ef}}$ on the macroscopic wave function is given in the space and time domains by the convolution

$$(\hat{H}_{\text{ef}}\Psi)(\mathbf{r},t) = \int d^N\mathbf{r}' \int_0^t dt'\, H_{\text{ef}}(\mathbf{r} - \mathbf{r}',t - t')\Psi(\mathbf{r}',t'). \tag{7}$$

The Fourier transform of the kernel $H_{\text{ef}}(\mathbf{r},t)$ is denoted by $H_{\text{ef}}(\mathbf{k},\omega) = \int d^N\mathbf{r}\int_0^\infty dt\, H_{\text{ef}}(\mathbf{r},t)\,e^{i\omega t}e^{-i\mathbf{k}\cdot\mathbf{r}}$. Clearly, the function $H_{\text{ef}}(\mathbf{k},\omega)$ completely determines the effective Hamiltonian. To obtain an explicit formula for $H_{\text{ef}}(\mathbf{k},\omega)$, we calculate the unilateral Laplace transform of the Schrödinger equation (1) to find that

$$(\hat{H} - E)\psi(\mathbf{r},\omega) = -i\hbar\psi_{t=0}(\mathbf{r}), \tag{8}$$

with $E = \hbar\omega$. Thus, applying the spatial averaging operator to both sides of the equation and using (6), it follows that for an initial macroscopic state:

$$(H_{\text{ef}}\Psi)(\mathbf{r},\omega) - E\Psi(\mathbf{r},\omega) = -i\hbar\psi_{t=0}(\mathbf{r}). \tag{9}$$

Let us now consider the particular case wherein the initial state is $\psi_{t=0}(\mathbf{r}) \sim e^{i\mathbf{k}\cdot\mathbf{r}}$. Clearly, in these conditions the solution of Eq. (8) has the $\mathbf{k}$-Bloch property. Functions with the Bloch property, with $\mathbf{k}$ in the BZ, have spatial averages of the form [18]

$$\Psi(\mathbf{r}) = \psi_{\text{av}}e^{i\mathbf{k}\cdot\mathbf{r}}, \tag{10}$$

where

$$\psi_{\text{av}} = \frac{1}{V_c}\int_\Omega \psi(\mathbf{r})e^{-i\mathbf{k}\cdot\mathbf{r}}d^N\mathbf{r}, \tag{11}$$

where V_c is the volume of the unit cell Ω in the spatial domain. This property and Eq. (7) imply that $(\hat{H}_{\text{ef}}\Psi)(\mathbf{r},\omega) = H_{\text{ef}}(\mathbf{k},\omega)\Psi(\mathbf{r},\omega)$ and hence from Eq. (6) we get

$$H_{\text{ef}}(\mathbf{k},\omega)\Psi(\mathbf{r},\omega) = \{(\hat{H}\psi)(\mathbf{r},\omega)\}_{\text{av}}. \tag{12}$$

Hence, by numerically solving Eq. (8) with respect to ψ for the initial macroscopic state $\psi_{t=0}(\mathbf{r}) \sim e^{i\mathbf{k}\cdot\mathbf{r}}$ and feeding the result to Eq. (12), it is possible to compute the unknown function $H_{\text{ef}}(\mathbf{k},\omega)$ for any value of $(\mathbf{k},\omega)$. Note that $(\hat{H}\psi)(\mathbf{r},\omega)$ has the $\mathbf{k}$-Bloch property, and hence $\{(\hat{H}\psi)(\mathbf{r},\omega)\}_{\text{av}}$ can be obtained using a formula analogous to Eq. (10).

One interesting property of the effective Hamiltonian is that the solutions of

$$\det(H_{\text{ef}}(\mathbf{k},\omega) - E) = 0 \tag{13}$$

yield the exact energy band structure of the original microscopic Hamiltonian. For more details the reader is referred to Ref. [18]. In previous works, this general formalism was applied to graphene and semiconductor superlattices in different contexts [20–22,30,31]. Moreover, related effective medium techniques have been widely used to model the propagation of light in electromagnetic metamaterials [32–35].

B. Single-component Hamiltonian

Next, we apply the formalism described in the previous section to characterize a 2DEG under the action of a periodic electrostatic potential $V(\mathbf{r})$ with the honeycomb symmetry.
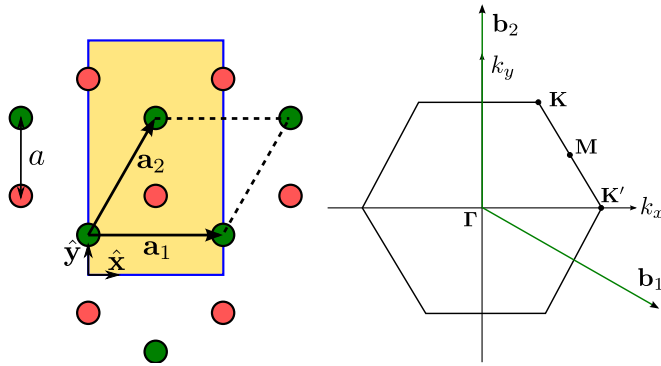
FIG. 1. (Color online) (Left) 2DEG modulated by an applied potential with the honeycomb symmetry. A primitive cell is delimited by the dotted lines. The supercell used in the FDFD numerical calculations is represented by the colored area. (Right) First Brillouin zone with the usual high-symmetry points.

Similar to Ref. [17], it is assumed that the system corresponds to a modulation-doped GaAs/AlGaAs quantum well. The geometry of the patterned 2DEG is represented in Fig. 1 (left). It is assumed that the electric potential is a constant V_0 inside each disk of radius R, and zero outside. A primitive cell of the honeycomb lattice, with primitive vectors $\mathbf{a}_1$ and $\mathbf{a}_2$, is delimited in the figure by the dotted lines. This primitive cell contains two inequivalent elements each represented by a different color. The spacing between nearest neighbors is denoted by a. For the numerical calculations, it is convenient to consider as well a rectangular supercell containing four elements (yellow region). The primitive vectors of the reciprocal lattice, $\mathbf{b}_1$ and $\mathbf{b}_2$, are represented in Fig. 1 (right) together with the first Brillouin zone and with some relevant high-symmetry points.

The microscopic Hamiltonian for this two-dimensional system is simply

$$\hat{H} = \frac{-\hbar^2}{2m_b}\nabla^2 + V(\mathbf{r}), \tag{14}$$

where the electron effective mass m_b is taken as in Ref. [17]: $m_b = 0.067m$, with m the electron rest mass. This Hamiltonian for a 2DEG of noninteracting electrons is the starting point of our first-principles effective medium theory.

As outlined in Sec. II A, the first step to compute the effective Hamiltonian $H_{\text{ef}}(\mathbf{k},\omega)$ is to find the microscopic wave function $\psi(\mathbf{r},\omega)$ that satisfies Eq. (8) for a macroscopic initial state $-i\hbar\psi_{t=0}(\mathbf{r}) = f_0 e^{i\mathbf{k}\cdot\mathbf{r}}$ where f_0 is an arbitrary constant (the effective Hamiltonian is independent of the value of f_0). Equation (8) is numerically solved for a fixed $(\mathbf{k},\omega)$ using the finite-difference frequency domain (FDFD) method. The details can be found in Appendix A 1. From the knowledge of $\psi(\mathbf{r},\omega)$, the effective Hamiltonian $H_{\text{ef}}(\mathbf{k},\omega)$ is deduced as follows. Substituting the identity $(\hat{H}_{\text{ef}}\Psi)(\mathbf{r},\omega) = H_{\text{ef}}(\mathbf{k},\omega)\Psi(\mathbf{r},\omega)$ and Eq. (10) into Eq. (9), it follows that

$$(H_{\text{ef}}(\mathbf{k},\omega) - E)\psi_{\text{av}}(\mathbf{k},\omega)e^{i\mathbf{k}\cdot\mathbf{r}} = f_0 \cdot e^{i\mathbf{k}\cdot\mathbf{r}}, \tag{15}$$

where $\psi_{\text{av}}(\mathbf{k},\omega)$ is defined as in Eq. (11) where V_c should be understood as the area of the unit cell. Thus, because the single-component effective Hamiltonian corresponds to a multiplication operator in the spectral domain, it may be
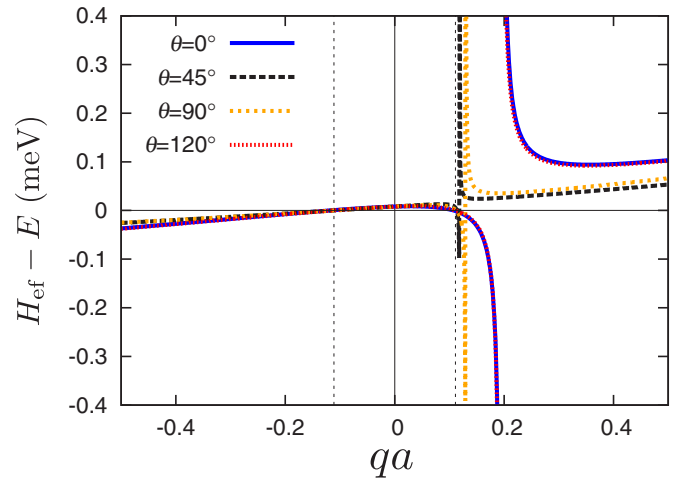

FIG. 2. (Color online) Plot of the single-component effective Hamiltonian H_{ef} near the K point as a function of the normalized wave vector for different directions of propagation and $E = -0.33$ meV, $N_x = 97$, $N_y = 117$, $V_0 = -0.8$ meV, and $R/a = 0.35$. The vertical dashed lines indicate the zeros of $H_{\text{ef}} - E$.

expressed as

$$H_{\text{ef}}(\mathbf{k},\omega) = f_0 \cdot \psi_{\text{av}}^{-1}(\mathbf{k},\omega) + E. \tag{16}$$

To give an example, we suppose that the structural parameters are such that $V_0 = -0.8$ meV, $R/a = 0.35$, and $a = 150$ nm. The electronic band structure for this system was reported in Ref. [17], and hence it will not be repeated here. As discussed in Ref. [17], for an attractive potential it is possible to have an electronic band structure with isolated Dirac points. For the chosen structural parameters, the tip of the Dirac cone at the K point occurs at the energy level $E_D = -0.326$ meV. Because we are interested in the physics near the K point, it is implicitly assumed that BZ in Eq. (4) represents the translation of the first Brillouin zone to the K point.

In Fig. 2, we depict the calculated scalar effective Hamiltonian H_{ef} for the energy $E = -0.33$ meV. In the numerical simulations we used a grid with $N_x \times N_y = 97 \times 117$ points. The effective Hamiltonian H_{ef} is represented as a function of the wave vector measured with respect to the K point, so that $\mathbf{q} = \mathbf{k} - \mathbf{K}$. The function plotted in the figure is $H_{\text{ef}} - E$ versus the magnitude of the normalized wave vector for different directions of propagation. The angle θ is the angle between $\mathbf{q}$ and the k_x axis (see Fig. 1).

As seen, for every direction θ, the function $H_{\text{ef}} - E$ intersects the horizontal axis at exactly one point (here, negative values of q are understood as being calculated for the opposite direction $\theta + \pi$). Moreover, the position of the zeros is nearly independent of the angle θ. This is consistent with the fact that the solutions of Eq. (13) give the dispersion of the stationary states, which for a graphenelike system, due to the isotropy, should depend only on q and not on θ. Importantly, Fig. 2 also demonstrates that the effective Hamiltonian H_{ef} depends strongly on $\mathbf{q}$, and that it can have pole singularities for some specific values $\mathbf{q}$. This means that the time evolution operator is strongly spatially dispersive. In other words, the inverse Fourier transform in $\mathbf{k}$ of $H_{\text{ef}}(\mathbf{k},\omega)$ is spread over a wide region of space, which implies that the action of the effective

Hamiltonian on Ψ is nonlocal. This property is undesired because the associated formalism is impractical and lacks elegance. In the next section, we prove that by considering a modified effective medium approach wherein the averaged wave function is described by a pseudospinor it is possible to overcome these problems.

III. TWO-COMPONENT HAMILTONIAN FOR A POTENTIAL WITH THE HONEYCOMB SYMMETRY

The nonlocal spatial action of the single-component effective Hamiltonian can be attributed to the fact that the electron wave function can have significant fluctuations within each unit cell because the system is formed by two inequivalent sublattices, i.e., that there are two inequivalent elements per unit cell. This observation suggests that our definition of macroscopic state may be too restrictive for this system, because it does not allow us to consider electronic states that are more localized than the unit cell, and hence the two sublattices are not discriminated. As demonstrated in the following, it is possible to avoid these problems by extending the definition of macroscopic states.

A. Two components effective Hamiltonian

To begin with, let us decompose the crystal into two regions, each described by a characteristic function $\chi_i(\mathbf{r})$ ($i = 1,2$) such that $\chi_1(\mathbf{r}) + \chi_2(\mathbf{r}) = 1$. Specifically, the characteristic functions are chosen such that $\chi_i(\mathbf{r})$ delimits a triangle centered on each disk of the same type and is equal to 1 in the region ① and 0 in the complementary region (see Fig. 3 and compare with the supercell represented in Fig. 1). Note that this partition can be obtained through a process similar to the one used to construct the Wigner-Seitz cell, but rather than picking neighbor lattice points one picks elements from different sublattices. Hence $\chi_i(\mathbf{r})$ are the characteristic functions associated with the two sublattices of the crystal.

Based on this decomposition, we introduce the notion of *generalized* macroscopic state, as a state that can be decomposed as $\psi(\mathbf{r}) = \chi_1(\mathbf{r})\psi_1(\mathbf{r}) + \chi_2(\mathbf{r})\psi_2(\mathbf{r})$ for some functions ψ_i ($i = 1,2$) with $\psi_i(\mathbf{r}) = \{\psi_i(\mathbf{r})\}_{\text{av}}$. Clearly, this definition generalizes that of Sec. II A. The idea is now to introduce a generalized effective Hamiltonian that allows us
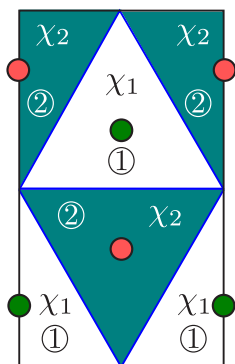

FIG. 3. (Color online) Representation of the $\chi_i(\mathbf{r})$ function that generates the pseudospinor wave function Φ.

to characterize the time evolution of generalized macroscopic states.

To this end, we introduce a pseudospinor given by

$$\Phi = \begin{pmatrix} \Phi_1 \\ \Phi_2 \end{pmatrix} = \begin{pmatrix} \psi\chi_1 \\ \psi\chi_2 \end{pmatrix}. \tag{17}$$

This decomposition is inspired by the well known property that each component of the pseudospinor in graphene is associated with a specific sublattice of the material [2]. We note that $\psi = \Phi_1 + \Phi_2$, and thus from the microscopic Schrödinger equation (1) it is possible to write

$$(\chi_1 + \chi_2)\left(\hat{H} - i\hbar\frac{\partial}{\partial t}\right)(\Phi_1 + \Phi_2) = 0, \tag{18}$$

This scalar equation is equivalent to the matrix system

$$\underbrace{\begin{pmatrix} \chi_1\hat{H}\chi_1 & \chi_1\hat{H}\chi_2 \\ \chi_2\hat{H}\chi_1 & \chi_2\hat{H}\chi_2 \end{pmatrix}}_{\hat{H}_g} \cdot \Phi = i\hbar\frac{\partial}{\partial t}\Phi, \tag{19}$$

where $\hat{H}_g$ is a generalized two-component microscopic Hamiltonian. We want to obtain an effective medium description of the above time evolution problem with the macroscopic state given by the spatially averaged pseudospinor Φ.

To this end, assuming an initial generalized macroscopic state of the form $\psi_{t=0}(\mathbf{r}) = \chi_1(\mathbf{r})\psi_{1,t=0}(\mathbf{r}) + \chi_2(\mathbf{r})\psi_{2,t=0}(\mathbf{r})$, we calculate the Laplace transform of Eq. (19) to obtain

$$(\hat{H}_g - E) \cdot \Phi(\mathbf{r},\omega) = \begin{pmatrix} -i\hbar\,\psi_{1,t=0}\,\chi_1 \\ -i\hbar\,\psi_{2,t=0}\,\chi_2 \end{pmatrix}. \tag{20}$$

The effective Hamiltonian operator $\hat{H}_{g,\text{ef}}$ is defined so that $(\hat{H}_{g,\text{ef}}\{\Phi\}_{\text{av}})(\mathbf{r},t) = \{(\hat{H}_g\Phi)(\mathbf{r},t)\}_{\text{av}}$ for any initial generalized macroscopic state [compare with Eq. (5)]. To find an explicit formula for $\hat{H}_{g,\text{ef}}(\mathbf{k},\omega)$ in the Fourier domain, we follow the same steps as in Sec. II A. Assuming that the initial state is such that $-i\hbar\,\psi_{i,t=0}(\mathbf{r}) = f_i e^{i\mathbf{k}\cdot\mathbf{r}}$ ($i = 1,2$), with the weights f_i generic constants, it is simple to prove that

$$(H_{g,\text{ef}}(\mathbf{k},\omega) - E) \cdot \{\Phi\}_{\text{av}}$$
$$= f_1 \left\{ \begin{pmatrix} \chi_1 \\ 0 \end{pmatrix} e^{i\mathbf{k}\cdot\mathbf{r}} \right\}_{\text{av}} + f_2 \left\{ \begin{pmatrix} 0 \\ \chi_2 \end{pmatrix} e^{i\mathbf{k}\cdot\mathbf{r}} \right\}_{\text{av}}, \tag{21}$$

where $\{\Phi\}_{\text{av}}$ is defined as

$$\{\Phi\}_{\text{av}} = \left(\frac{1}{V_c}\int \Phi(\mathbf{r},\omega) \cdot e^{-i\mathbf{k}\cdot\mathbf{r}} d^N\mathbf{r}\right) e^{i\mathbf{k}\cdot\mathbf{r}}$$
$$= \Phi_{\text{av}} e^{i\mathbf{k}\cdot\mathbf{r}}. \tag{22}$$

Because the volume fraction of the two regions is identical, we have

$$\left\{ \begin{pmatrix} \chi_1 \\ 0 \end{pmatrix} e^{i\mathbf{k}\cdot\mathbf{r}} \right\}_{\text{av}} = \left(\frac{1}{V_c}\int \chi_1(\mathbf{r})d^N\mathbf{r}\right)\begin{pmatrix} 1 \\ 0 \end{pmatrix}e^{i\mathbf{k}\cdot\mathbf{r}} = \frac{1}{2}\begin{pmatrix} 1 \\ 0 \end{pmatrix}e^{i\mathbf{k}\cdot\mathbf{r}}. \tag{23}$$

Thus Eq. (21) becomes

$$[H_{g,\text{ef}}(\mathbf{k},\omega) - E] \cdot \Phi_{\text{av}} = f_1\frac{1}{2}\begin{pmatrix} 1 \\ 0 \end{pmatrix} + f_2\frac{1}{2}\begin{pmatrix} 0 \\ 1 \end{pmatrix}. \tag{24}$$

Let now $\Phi^{(1)}$ and $\Phi^{(2)}$ be the two independent solutions of (20), corresponding respectively to $f_1 = 1$, $f_2 = 0$ and $f_1 = 0$,

$f_2 = 1$. Then, it is possible to write the matrix equation

$$[H_{g,\mathrm{ef}}(\mathbf{k},\omega) - E] \cdot \begin{pmatrix} \Phi_{\mathrm{av}}^{(1)} & \Phi_{\mathrm{av}}^{(2)} \end{pmatrix} = \frac{1}{2}\begin{pmatrix} 1 & 0 \\ 0 & 1 \end{pmatrix}, \qquad (25)$$

or equivalently,

$$H_{g,\mathrm{ef}}(\mathbf{k},\omega) = E + \frac{1}{2}\begin{pmatrix} \Phi_{\mathrm{av}}^{(1)} & \Phi_{\mathrm{av}}^{(2)} \end{pmatrix}^{-1}. \qquad (26)$$

In summary, we demonstrated that the two component effective Hamiltonian can be written in terms of the functions $\Phi^{(i)}$ ($i = 1,2$) as shown above. From the definition, $\Phi^{(i)}$ satisfies Eq. (20) with $-i\hbar\,\psi_{j,t=0} = \delta_{i,j}e^{i\mathbf{k}\cdot\mathbf{r}}$ ($j = 1,2$). It is easy to check that it can be written as

$$\Phi^{(i)} = \begin{pmatrix} \psi^{(i)}\chi_1 \\ \psi^{(i)}\chi_2 \end{pmatrix}, \qquad (27)$$

where $\psi^{(i)}$ ($i = 1,2$) is the solution of the scalar problem

$$(\hat{H} - E)\psi^{(i)} = \chi_i e^{i\mathbf{k}\cdot\mathbf{r}}. \qquad (28)$$

Thus, to compute the two-component Hamiltonian $H_{g,\mathrm{ef}}(\mathbf{k},\omega)$, one needs to solve two independent scalar problems. This operator describes exactly the time evolution of any generalized macroscopic state with a pseudospinor formalism.

B. Single-component Hamiltonian obtained from the pseudospinor formalism

It should be clear from the previous section that $H_{g,\mathrm{ef}}$ is a generalization of H_{ef} defined in Sec. II. This suggests that H_{ef} can be written in terms of $H_{g,\mathrm{ef}}$. In the following, we obtain the explicit relation between the two Hamiltonians.

To begin with, we note that solving Eq. (8) for a macroscopic initial state $-i\hbar\,\psi_{t=0}(\mathbf{r}) = f_0 e^{i\mathbf{k}\cdot\mathbf{r}}$ is equivalent to solve Eq. (20) with an initial state $-i\hbar\,\psi_{i,t=0}(\mathbf{r}) = f_i e^{i\mathbf{k}\cdot\mathbf{r}}$ ($i = 1,2$) with $f_1 = f_2 = f_0$. Fixing $f_1 = f_2 = f_0$ in Eq. (24), we find after straightforward manipulations that for such an excitation

$$\Phi_{\mathrm{av}} = \frac{f_0}{2}[H_{g,\mathrm{ef}}(\mathbf{k},\omega) - E]^{-1} \cdot \begin{pmatrix} 1 \\ 1 \end{pmatrix}. \qquad (29)$$

Then, noting that $\psi_{\mathrm{av}} = \Phi_{1,\mathrm{av}} + \Phi_{2,\mathrm{av}}$, it follows that

$$\psi_{\mathrm{av}} = \frac{f_0}{2}\sum_{i,j}[(H_{g,\mathrm{ef}}(\mathbf{k},\omega) - E)^{-1}]_{i,j}, \qquad (30)$$

and thus, by substitution into Eq. (16), the single-component Hamiltonian $\hat{H}_{\mathrm{ef}}^{(s)}$ deduced from $\hat{H}_{g,\mathrm{ef}}$ is

$$H_{\mathrm{ef}}^{(s)}(\mathbf{k},\omega) = \frac{2}{\sum_{i,j}[(H_{g,\mathrm{ef}}(\mathbf{k},\omega) - E)^{-1}]_{i,j}} + E. \qquad (31)$$

We numerically verified that $H_{\mathrm{ef}}^{(s)}$ given by the above formula is exactly coincident with scalar effective Hamiltonian, $\hat{H}_{\mathrm{ef}}$, obtained with the calculation method described in Sec. II, as it should be. This coincidence supports the correctness of our numerical codes.

It is interesting to note that Eq. (31) explicitly shows that the zeros of $H_{\mathrm{ef}}^{(s)}(\mathbf{k},\omega) - E$ occur for the same values of $(\mathbf{k},\omega)$ as the poles of $(H_{g,\mathrm{ef}}(\mathbf{k},\omega) - E)^{-1}$. This is equivalent to say that the zeros of $H_{\mathrm{ef}}(\mathbf{k},\omega) - E$ are coincident with the zeros of $\det(H_{g,\mathrm{ef}}(\mathbf{k},\omega) - E)$. This is a consequence of the fact that the electronic band structure of the microscopic

Hamiltonian is exactly predicted by the two effective medium formulations [18].

C. Stationary states near the K point

As mentioned in section II A, the stationary electronic states of the 2DEG can be obtained from the pseudospinor effective Hamiltonian $H_{g,\mathrm{ef}}$ by finding the solutions of

$$\det(H_{g,\mathrm{ef}}(\mathbf{k},E) - E) = 0. \qquad (32)$$

In this work, we are mainly interested in the physics near the high-symmetry $\mathbf{K}$ point. Hence, it is convenient to simplify the formalism and use an analytical approximation for $H_{g,\mathrm{ef}}$ to solve the secular equation. For electron states with the spatial spectrum concentrated near the $\mathbf{K}$ point, we can approximate $H_{g,\mathrm{ef}}$ by its Taylor series:

$$H_{g,\mathrm{ef}}(\mathbf{k},E) \simeq H_{g,\mathrm{ef}}(\mathbf{K},E) + \frac{\partial H_{g,\mathrm{ef}}(\mathbf{k},E)}{\partial k_x}\bigg|_{\mathbf{k}=\mathbf{K}} q_x$$
$$+ \frac{\partial H_{g,\mathrm{ef}}(\mathbf{k},E)}{\partial k_y}\bigg|_{\mathbf{k}=\mathbf{K}} q_y, \qquad (33)$$

with k_x, k_y, and q_x, q_y the components of the wave vectors $\mathbf{k}$ and $\mathbf{q} = \mathbf{k} - \mathbf{K}$, respectively. In practice, the derivatives of the effective Hamiltonian are numerically evaluated with finite differences. The band energy diagram $E(\mathbf{k})$ of the system is then obtained by solving (32) using the approximate expression of $H_{g,\mathrm{ef}}(\mathbf{k},E)$. Notably, we numerically verified that the two component Hamiltonian is a smooth slowly-varying function of $\mathbf{q}$ (not shown), and hence the above Taylor expansion is typically a quite good approximation for the Hamiltonian. This contrasts with the singular behavior of the single-component effective Hamiltonian (see Fig. 2).

The energy dispersion diagrams obtained with this approach for a system with the same parameters as in Fig. 2 ($R/a = 0.35$ and $V_0 = -0.8$ meV) are depicted in Fig. 4 (dashed lines). Each plot corresponds to a specific angle of propagation θ, with θ defined in the same way as in Fig. 2. The solid lines correspond to the exact electronic band structure, and were obtained with the plane wave method [17,36,37] by solving

$$\det\left[\left(\frac{\hbar^2}{2m}(\mathbf{k} - \mathbf{G})^2 - E(\mathbf{k})\right)\delta_{\mathbf{G},\mathbf{G}'} + \tilde{V}(\mathbf{G}' - \mathbf{G})\right] = 0, \qquad (34)$$

where $\mathbf{G}$, $\mathbf{G}'$ are the reciprocal lattice vectors and $\tilde{V}$ is the Fourier transform of the potential. As seen in Fig. 4, there is a very good agreement between the plane-wave method and the effective medium results near the K point for all the directions of propagation. Note that the results are not exactly coincident because of the approximation implicit in the Taylor expansion of $H_{g,\mathrm{ef}}$ near the K point. However, the proximity between the two sets of curves confirms that Eq. (33) is, indeed, quite accurate. Moreover, our effective medium results corroborate the findings of Ref. [17]: near the K point, the energy dispersion diagrams are linear, isotropic, with a zero band gap. These properties are not the only similarities of the modulated 2DEG with graphene. In fact, we shall prove in the following that the electronic states pseudospinor may also be determined by a 2D massless Dirac fermion Hamiltonian
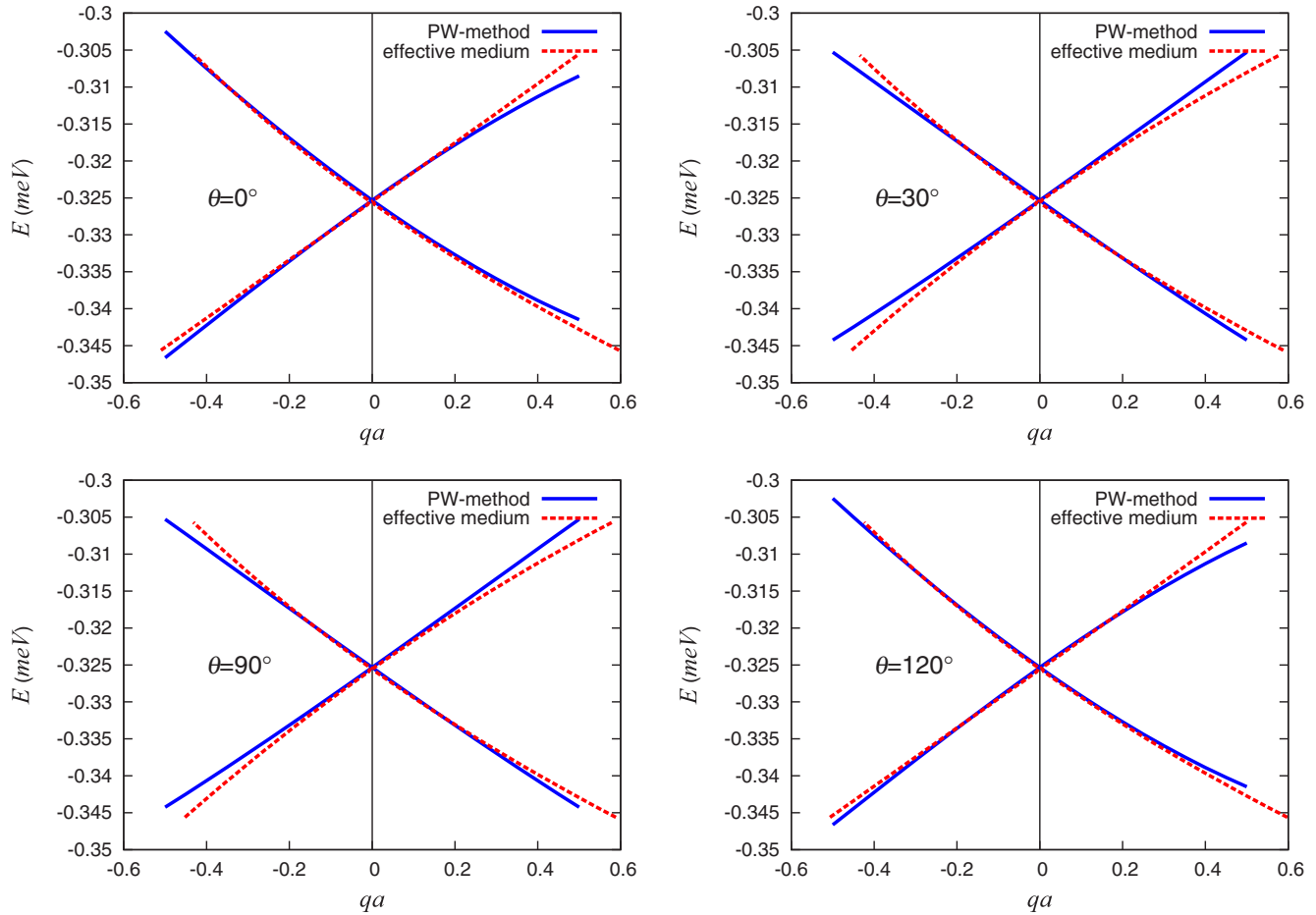
FIG. 4. (Color online) Electronic band structure near the K point for different propagation directions and for a modulated 2DEG with a potential $V_0 = -0.8$ meV, a ratio $R/a = 0.35$, and a number of nodes in the FDFD grid $N_x = 97$ and $N_y = 117$. Dashed red lines: calculated with the two-component effective Hamiltonian. Solid blue lines: calculated with the plane wave method.

$\hat{H}_D = \hbar v_F \boldsymbol{\sigma} \cdot \mathbf{q}$, where v_F is the equivalent "Fermi velocity" and $\boldsymbol{\sigma}$ are the Pauli matrices. However, a renormalization of the pseudospinor is required. The reason is discussed in the next sections.

D. Macroscopic probability density for the stationary states

The probability density function is of fundamental importance in quantum mechanics since it is essential to make physical predictions. Within the usual microscopic framework, it is given by $\mathcal{P}_{\text{mic}} = \psi^* \cdot \psi$. Evidently, it can also be written in terms of the pseudospinor (17) as $\mathcal{P}_{\text{mic}} = \Phi^* \cdot \Phi$. Hence the average probability density for a Bloch wave is

$$\mathcal{P}_{\text{mic,av}} = \{\Phi^* \cdot \Phi\}_{\text{av}} = \frac{1}{V_c} \int \Phi^* \cdot \Phi \, d^N \mathbf{r}. \quad (35)$$

One important observation is that, in general, the averaging operation does not commute with multiplication operation

$$\{\Phi^* \cdot \Phi\}_{\text{av}} \neq \{\Phi\}_{\text{av}}^* \cdot \{\Phi\}_{\text{av}}. \quad (36)$$

This indicates that in general the squared amplitude of the spatially averaged wave function cannot be identified with the probability density in the macroscopic framework. This may look peculiar at first sight, but actually the situation is quite analogous to what happens in macroscopic electrodynamics

wherein the formula for the stored energy calculated using the macroscopic electromagnetic fields differs from the formula for the stored energy calculated using the microscopic fields [29,38].

It is demonstrated in Appendix B (see also the supplementary materials of Ref. [31]) that for stationary (Bloch) electronic states the following relation holds exactly:

$$\{\Phi^* \cdot \Phi\}_{\text{av}} = 2 \{\Phi\}_{\text{av}}^* \cdot \left(\mathbf{1} - \frac{\partial \hat{H}_{g,\text{ef}}(\mathbf{k}, E)}{\partial E}\right) \cdot \{\Phi\}_{\text{av}}. \quad (37)$$

Hence, we can write

$$\mathcal{P}_{\text{mic,av}} = \mathcal{P}_{\text{mac}}, \quad (38)$$

where the macroscopic probability density is defined as

$$\mathcal{P}_{\text{mac}} = 2 \{\Phi\}_{\text{av}}^* \cdot \left(\mathbf{1} - \frac{\partial \hat{H}_{g,\text{ef}}(\mathbf{k}, E)}{\partial E}\right) \cdot \{\Phi\}_{\text{av}}. \quad (39)$$

Thus the formula for the macroscopic probability density differs from that of the microscopic probability density.

For convenience, we define the Dirac energy, E_D, as the energy for which the valence and conduction bands coincide. Interestingly, our numerical calculations indicate that near the Dirac energy $\mathbf{1} - \frac{\partial \hat{H}_{g,\text{ef}}(\mathbf{k}, E)}{\partial E}$ varies slowly. Thus the
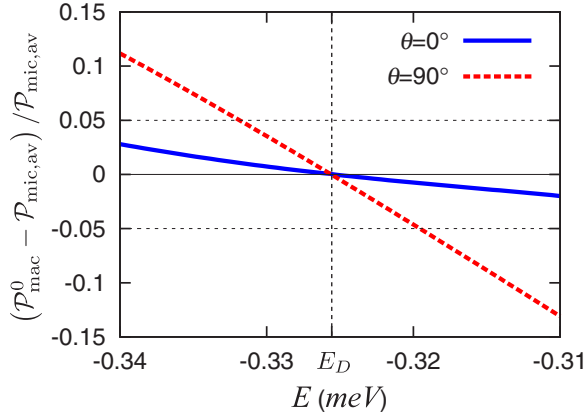
FIG. 5. (Color online) Relative difference between $\mathcal{P}_{\text{mic,av}}$ and $\mathcal{P}_{\text{mac}}^0$ as a function of energy for a modulated 2DEG with the same parameters as in Fig. 4. Two different directions of propagation are considered.

macroscopic probability density may be approximated by

$$\mathcal{P}_{\text{mac}} \approx \mathcal{P}_{\text{mac}}^0 = 2 \{\Phi\}_{\text{av}}^* \cdot \mathbf{A}_0 \cdot \{\Phi\}_{\text{av}}, \qquad (40)$$

with $\mathbf{A}_0 = \mathbf{1} - \frac{\partial \hat{H}_{g,\text{ef}}(\mathbf{k},E)}{\partial E}|_{E=E_D,\mathbf{k}=\mathbf{K}}$.

To confirm the validity of this formula, we numerically calculated the relative difference between $\mathcal{P}_{\text{mic,av}}$ and $\mathcal{P}_{\text{mac}}^0$ for the stationary states of the system near E_D and for two directions of propagation θ. As seen in Fig. 5, in the considered energy range, the error in the approximation is smaller than 15% for a direction of propagation with $\theta = 90°$, and smaller than 5% for $\theta = 0°$. Notice that the error vanishes at the Dirac energy because in this case $\mathcal{P}_{\text{mac}}$ is equal to $\mathcal{P}_{\text{mac}}^0$, and from Eq. (37) the relative difference between the probability densities is exactly zero at this point. We also verified (not shown) that within numerical precision, $\mathcal{P}_{\text{mic,av}} = \mathcal{P}_{\text{mac}}$ for all energy values.

E. Massless Dirac equation

We are now ready to show that the modulated 2DEG may be described by the massless Dirac equation. The starting point is to generalize Eq. (33) and expand the effective Hamiltonian in the spectral domain in a Taylor series near E_D and $\mathbf{K}$ so that

$$(\hat{H}_{g,\text{ef}} - E) \cdot \{\Phi\}_{\text{av}} \simeq -(E - E_D)\mathbf{A}_0 \cdot \{\Phi\}_{\text{av}} + q_x\mathbf{A}_1 \cdot \{\Phi\}_{\text{av}}$$
$$+ q_y\mathbf{A}_2 \cdot \{\Phi\}_{\text{av}}, \qquad (41)$$

where the matrix $\mathbf{A}_0$ is defined as in the previous section, $\mathbf{A}_1 = \frac{\partial \hat{H}_{g,\text{ef}}(\mathbf{k},E)}{\partial k_x}|_{E=E_D,\mathbf{k}=\mathbf{K}}$ and $\mathbf{A}_2 = \frac{\partial \hat{H}_{g,\text{ef}}(\mathbf{k},E)}{\partial k_y}|_{E=E_D,\mathbf{k}=\mathbf{K}}$. Next, we introduce a renormalized pseudospinor

$$\Phi_D = \sqrt{2} \cdot \mathbf{A}_0^{1/2} \cdot \{\Phi\}_{\text{av}} e^{-i\mathbf{K}\cdot\mathbf{r}}, \qquad (42)$$

which from Eq. (40) is such that for stationary states the probability density is given by the squared amplitude of the renormalized pseudospinor $\mathcal{P}_{\text{mac}} \approx \Phi_D \cdot \Phi_D^*$. Note that the Hermitian $\mathbf{A}_0$ matrix is necessarily positive definite and is not unitary. The secular equation $(\hat{H}_{g,\text{ef}} - E) \cdot \{\Phi\}_{\text{av}} = 0$ is equivalent to $(\hat{H}_D - E) \cdot \Phi_D = 0$ with $(\hat{H}_D - E) = \mathbf{A}_0^{-1/2} \cdot (\hat{H}_{g,\text{ef}} - E) \cdot \mathbf{A}_0^{-1/2}$. Simple manipulations show that in the

spatial domain:

$$\hat{H}_D = E_D - i\left(\frac{\partial}{\partial x}\tilde{\mathbf{A}}_1 + \frac{\partial}{\partial y}\tilde{\mathbf{A}}_2\right), \qquad (43)$$

where $\tilde{\mathbf{A}}_1 = \mathbf{A}_0^{-1/2} \cdot \mathbf{A}_1 \cdot \mathbf{A}_0^{-1/2}$ and $\tilde{\mathbf{A}}_2 = \mathbf{A}_0^{-1/2} \cdot \mathbf{A}_2 \cdot \mathbf{A}_0^{-1/2}$. Interestingly, our numerical calculations reveal (see Appendix C) that $\tilde{\mathbf{A}}_1$ and $\tilde{\mathbf{A}}_2$ are of the form

$$\tilde{\mathbf{A}}_1 = \hbar v_F(\cos\phi \cdot \sigma_x - \sin\phi \cdot \sigma_y),$$
$$\tilde{\mathbf{A}}_2 = \hbar v_F(\sin\phi \cdot \sigma_x + \cos\phi \cdot \sigma_y), \qquad (44)$$

where $\phi \approx 60°$, v_F is some constant that depends on the structural parameters of the 2DEG, and $\sigma_x = \begin{pmatrix} 0 & 1 \\ 1 & 0 \end{pmatrix}$ and $\sigma_y = \begin{pmatrix} 0 & -i \\ i & 0 \end{pmatrix}$ are the usual Pauli matrices. Thus the operator $\hat{H}_D$ can be written in a compact form as

$$\hat{H}_D = E_D - i\hbar v_F\left(\frac{\partial}{\partial x'}\sigma_x + \frac{\partial}{\partial y'}\sigma_y\right), \qquad (45)$$

where $\frac{\partial}{\partial x'}$ and $\frac{\partial}{\partial y'}$ are the directional derivatives along the directions $\phi = 60°$ and $\phi = 60° + 90°$, respectively,

$$\frac{\partial}{\partial x'} = \cos\phi\frac{\partial}{\partial x} + \sin\phi\frac{\partial}{\partial y}$$
$$\frac{\partial}{\partial y'} = -\sin\phi\frac{\partial}{\partial x} + \cos\phi\frac{\partial}{\partial y}. \qquad (46)$$

Thus $\hat{H}_D$ is exactly the 2D massless Dirac Hamiltonian, and the renormalized pseudospinor associated with stationary states is a solution of the time-independent Dirac equation $(\hat{H}_D - E) \cdot \Phi_D = 0$. It should be noted that the original coordinate axes need to be rotated by $\phi = 60°$ to get an Hamiltonian operator consistent with that of graphene. Our honeycomb lattice is actually rotated by 30° with respect to the definition usually adopted for graphene [2]. It can be verified that after a suitable similarity transformation $\hat{H}_D$ assumes the usual form in the standard coordinate system of graphene.

We would like to underline that in order to obtain a 2D massless Dirac Hamiltonian it was essential to renormalize the pseudospinor such that for stationary states, $\mathcal{P}_{\text{mac}} \approx \Phi_D \cdot \Phi_D^*$, because only in these conditions the analogy with graphene is complete. Notably, without this renormalization the Hamiltonian $\hat{H}_{g,\text{ef}}$ is not equivalent to a massless 2D Dirac Hamiltonian.

To further explore the analogy with graphene, next we numerically confirm that each component of the pseudospinor corresponds to a state localized on a different sublattice of the 2DEG. The eigenfunctions of the Dirac Hamiltonian $\hat{H}_D$ in the conduction band are proportional to $\begin{pmatrix} 1 \\ e^{i\theta_{\mathbf{q}}} \end{pmatrix}$, where $\theta_{\mathbf{q}} = \phi + \arctan\left(\frac{q_y}{q_x}\right)$ and q_x, q_y are measured relatively to the Dirac point. Note that $\theta_{\mathbf{q}}$ depends on the rotation angle $\phi = 60°$ previously discussed. Hence the two components of the pseudospinor Φ_D are in phase for $\theta_{\mathbf{q}} = \phi$ and out of phase for $\theta_{\mathbf{q}} = \phi - \pi$. To verify the connection between the microscopic and the macroscopic theories, we numerically calculated the microscopic wave function associated with a wave vector $\mathbf{q}$ oriented along the directions $\theta_{\mathbf{q}} = 60°$ and $\theta_{\mathbf{q}} = -120°$. In the simulations, it was assumed that $R/a = 0.35$, $V_0 = -0.8$ meV, and that $E - E_D = -0.329$ meV.
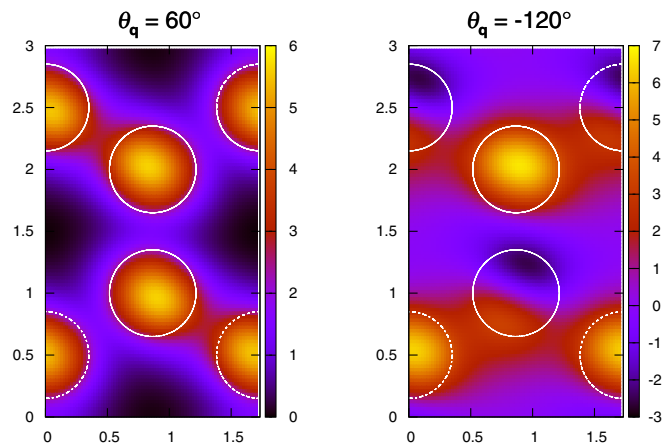
FIG. 6. (Color online) Density plot of $\mathrm{Re}[\frac{1}{\Phi_{1,\mathrm{av}}}\psi(\mathbf{r},\omega)e^{-i\mathbf{k}\cdot\mathbf{r}}]$ for $\theta_{\mathbf{q}} = 60°$ and $-120°$.

Figure 6 depicts the numerically calculated functions $\mathrm{Re}[\frac{1}{\Phi_{1,\mathrm{av}}}\psi(\mathbf{r},\omega)e^{-i\mathbf{k}\cdot\mathbf{r}}]$, i.e., the real part of the wave function envelope normalized to the first component $\Phi_{1,\mathrm{av}}$ of the pseudospinor $\{\Phi\}_{\mathrm{av}}$. The normalization to $\Phi_{1,\mathrm{av}}$ is done to ensure that the argument of the $\mathrm{Re}[\cdots]$ operator is dominantly real-valued. The white circles in Fig. 6 represent the positions of the disks where the potential is applied. One can see that for an angle of $\theta_{\mathbf{q}} = 60°$, the wave function envelope is in phase inside all disks, and therefore both components of the pseudospinor (17) are also in phase. On the contrary, for an angle of $\theta_{\mathbf{q}} = -120°$, the wave function envelope is out of phase inside the disks of the two different sublattices and thus the same is true for the components of the pseudospinor, as we wanted to show.

Up to now, the discussion was focused in the stationary states of the modulated 2DEG. Notably, the operator $\hat{H}_D$ also describes the time dynamics of generalized macroscopic states. This can be easily demonstrated by calculating the inverse Laplace-Fourier transform of the right-hand side of Eq. (41) and noting that for a time evolution problem it must vanish for $t > 0$. This yields

$$i\hbar \frac{\partial}{\partial t}\mathbf{A}_0 \cdot \tilde{\Phi}_{\mathrm{av}} = E_D \mathbf{A}_0 \cdot \tilde{\Phi}_{\mathrm{av}} - i\left(\frac{\partial}{\partial x}\mathbf{A}_1 + \frac{\partial}{\partial y}\mathbf{A}_2\right) \cdot \tilde{\Phi}_{\mathrm{av}},$$
$$t > 0, \qquad (47)$$

where $\tilde{\Phi}_{\mathrm{av}} = \{\Phi\}_{\mathrm{av}}\, e^{-i\mathbf{K}\cdot\mathbf{r}}$ is the envelope of the macroscopic wave function. Using now the definition of Φ_D [see Eq. (42)], it is easy to show that

$$i\hbar \frac{\partial \Phi_D}{\partial t} = \hat{H}_D \cdot \Phi_D, \qquad (48)$$

and hence the time evolution of generalized macroscopic states is indeed described by the massless 2D Dirac equation.

F. Parametric study

By varying the geometric parameters or the strength of the potential it is possible to tune the characteristics of the Dirac cones. Hence, it is useful to present a parametric study of the effective Hamiltonian parameters. Figures 7 and 8 show the dependance of the Dirac energy E_D, of the Fermi velocity

v_F and of the elements of the matrix $\mathbf{A}_0^{1/2}$ with the strength of the potential V_0 and with the normalized disk radius R/a, respectively. The range of values considered for V_0 is such that the only available stationary states near E_D are associated with the Dirac cones, in agreement with the study of Ref. [17].

First, we remark that the matrix $\mathbf{A}_0^{1/2}$ is an (almost diagonal) real-valued symmetric matrix whose elements remain almost constant when changing either the potential or the normalized radius R/a. Also, as expected, E_D becomes more negative as V_0 is decreased and as R/a is increased.

On the other hand, consistent with what is reported in Ref. [17], it is seen that the Fermi velocity increases as the absolute value of the potential is decreased, and exhibits a parabolic dependence on R/a. Moreover, the value of v_F is of the same order of magnitude as $v_F^{(nf)} = \frac{2\pi\hbar}{3\sqrt{3}m_b a} = 1.4\times10^4 \mathrm{~m\,s^{-1}}$ [17], which is roughly two orders of magnitude smaller than in graphene. Here, we would like to note that the value for $v_F^{(nf)}$ reported in Ref. [17] is overestimated by a factor of 10, likely due to a typo. Linear dispersing bands have exciting applications in terahertz photonics, and in the enhancement of the nonlinear optical response [8,22].

IV. HgCdTe HEXAGONAL SUPERLATTICE

In the second part of this paper, we apply the effective medium formalism to a different physical system with linearly dispersing bands. Specifically, in a previous work [22], we have shown how by combining mercury-cadmium-telluride (HgCdTe) semiconductor alloys it may be possible to realize a superlattice [19] with an isotropic zero-effective mass and a single valley linear energy-momentum dispersion near the Γ point. Here, we compute the effective Hamiltonian of the superlattice, and demonstrate that in this second platform the electrons do not have a pseudospin. HgCdTe quantum wells have recently elicited great attention in the context of the quantum spin Hall effect [39,40].

A. Microscopic Hamiltonian

The geometry of the heterostructure under study is depicted in Fig. 9. Similar to the previous sections, it is a two-dimensional structure (we are only interested in propagation in the xoy plane) formed by two lattice matched semiconductors. As discussed in Ref. [21], the physics of electron waves in binary compounds with a zinc-blende-type structure may be described by a potential V and by a dispersive (energy dependent) effective mass parameter m. In Fig. 9, the host material (in the exterior region) is characterized by parameters V_h and m_h, whereas the "disk"-type inclusions are characterized by the parameters V_i and m_i. As detailed below, V and m depend on the energy levels of the conduction and valence bands of each material. Consistent with the analysis of Refs. [21,22], and with the generalized Ben Daniel-Duke boundary conditions [23,24,41], this heterostructure may be modeled by a Hamiltonian $\hat{H}$ such that

$$\hat{H}\psi(\mathbf{r}) = \frac{-\hbar^2}{2}\nabla \cdot \left(\frac{1}{m(\mathbf{r})}\nabla\psi(\mathbf{r})\right) + V(\mathbf{r})\psi(\mathbf{r}). \qquad (49)$$
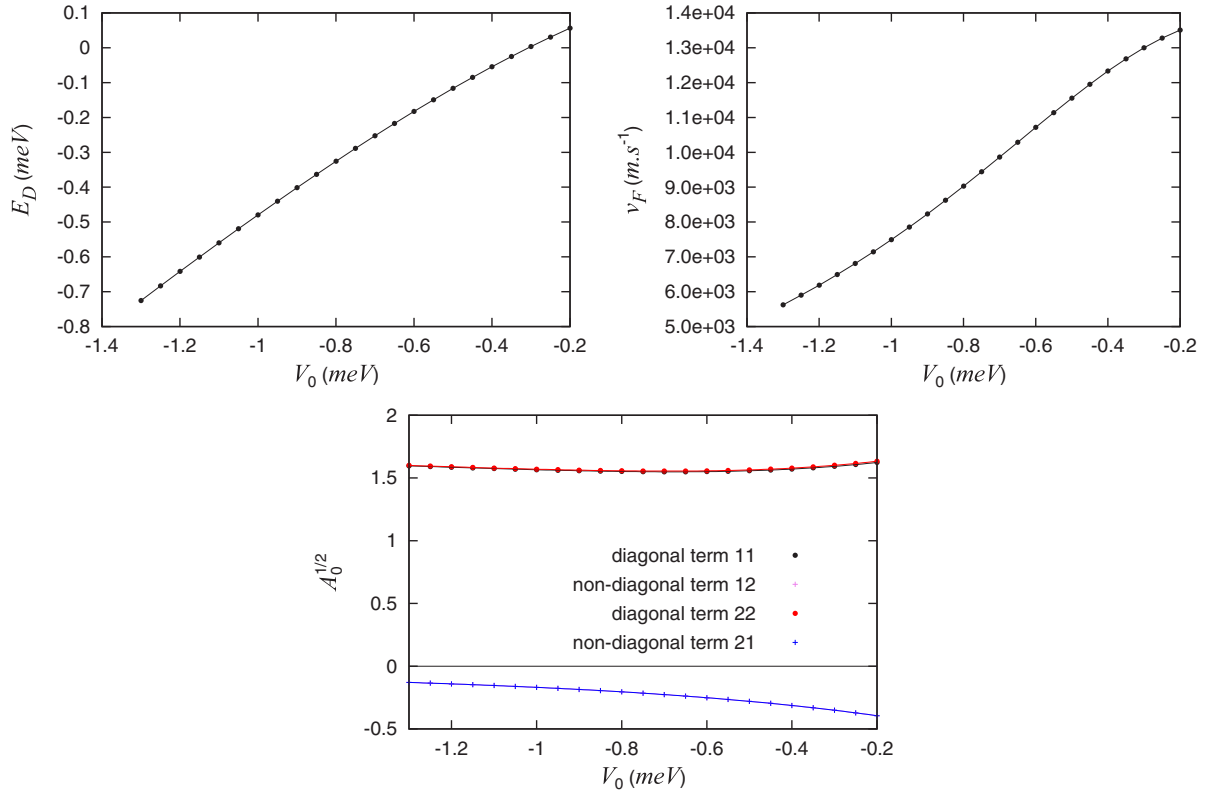
FIG. 7. (Color online) Dirac energy, Fermi velocity, and elements of the $\mathbf{A}_0^{1/2}$ matrix as a function of the potential V_0 obtained with the effective medium theory for the Dirac cone near the K point. In these simulations it was assumed that $R/a = 0.35$.

Similar to Ref. [22], we consider that the host material is $\text{Hg}_{0.75}\text{Cd}_{0.25}\text{Te}$ whereas the material of the inclusions is HgTe. These materials are nearly lattice matched. Note that unlike the 2DEG studied in the first part of the paper, the unit cell of the HgCdTe superlattice contains only one element.

Following Refs. [21,22,42] (see also Ref. [23]) for narrow gap binary compounds of the groups II-VI the potential V for each bulk material can be identified with the conduction band edge energy, $V(E) = E_c$, with $E_c = E_{\Gamma_6}$. On the other hand, the dispersive effective mass may be assumed to be of the form $m(E) = \frac{1}{2v_P^2}(E - E_v)$, with $E_v = E_{\Gamma_8}$ the energy level associated with the edge of the light-hole band and v_P the Kane's velocity.

For simplicity, here we assume that the elements of our 2D superlattice can be described by the same parameters as the corresponding bulk materials. Hence, for an $\text{Hg}_{0.75}\text{Cd}_{0.25}\text{Te}$-HgTe superlattice, V in Eq. (49) is such that

$$V_h = E_{v,h} + E_g(x = 0.25), \quad V_i = E_{v,i} + E_g(x = 0). \quad (50)$$

In the above, $E_g = E_g(x)$ stands for the band-gap energy of the ternary compound $\text{Hg}_x\text{Cd}_{1-x}\text{Te}$, which is calculated with Hansen's formula at zero temperature [43,44], where x represents the mole fraction. Notably, the electronic band structure of HgTe is inverted, so that the conduction (Γ_6) band (with an S-type symmetry) lies below the valence (Γ_8) band (with a P-type symmetry), and the band-gap energy is negative [20,45]. The valence band offset for the considered pair of

materials can be estimated equal to [21,22]

$$E_{v,h} = E_{v,i} - 0.0875 \text{ eV}. \quad (51)$$

The dispersive masses of the relevant semiconductors are

$$m_h = \frac{1}{2v_P^2}(E - E_{v,h}), \quad m_i = \frac{1}{2v_P^2}(E - E_{v,i}), \quad (52)$$

where the Kane velocity is supposed to be the same in the two media $v_P = 1.06 \times 10^6 \text{ m s}^{-1}$ [43].

B. Effective Hamiltonian and stationary states

The scalar effective Hamiltonian of the superlattice is computed in the same way as in Sec. II B. Now, BZ should be taken as the first Brillouin zone because for this superlattice the Dirac cone emerges at the Γ point [22]. The details of the numerical implementation of the FDFD method are described in Appendix A 2.

Interestingly, different from the example of Sec. II, our numerical calculations show that the effective Hamiltonian H_{ef} is a smooth function of $\mathbf{k}$ at the origin. Hence, it is possible to expand H_{ef} in a Taylor series in $\mathbf{k}$ as follows:

$$H_{\text{ef}}(\mathbf{k}, E) \simeq V_{\text{ef}}(E) + \frac{\hbar^2}{2}\mathbf{k} \cdot \overline{\overline{m}}_{\text{ef}}^{-1}(E) \cdot \mathbf{k}, \quad (53)$$
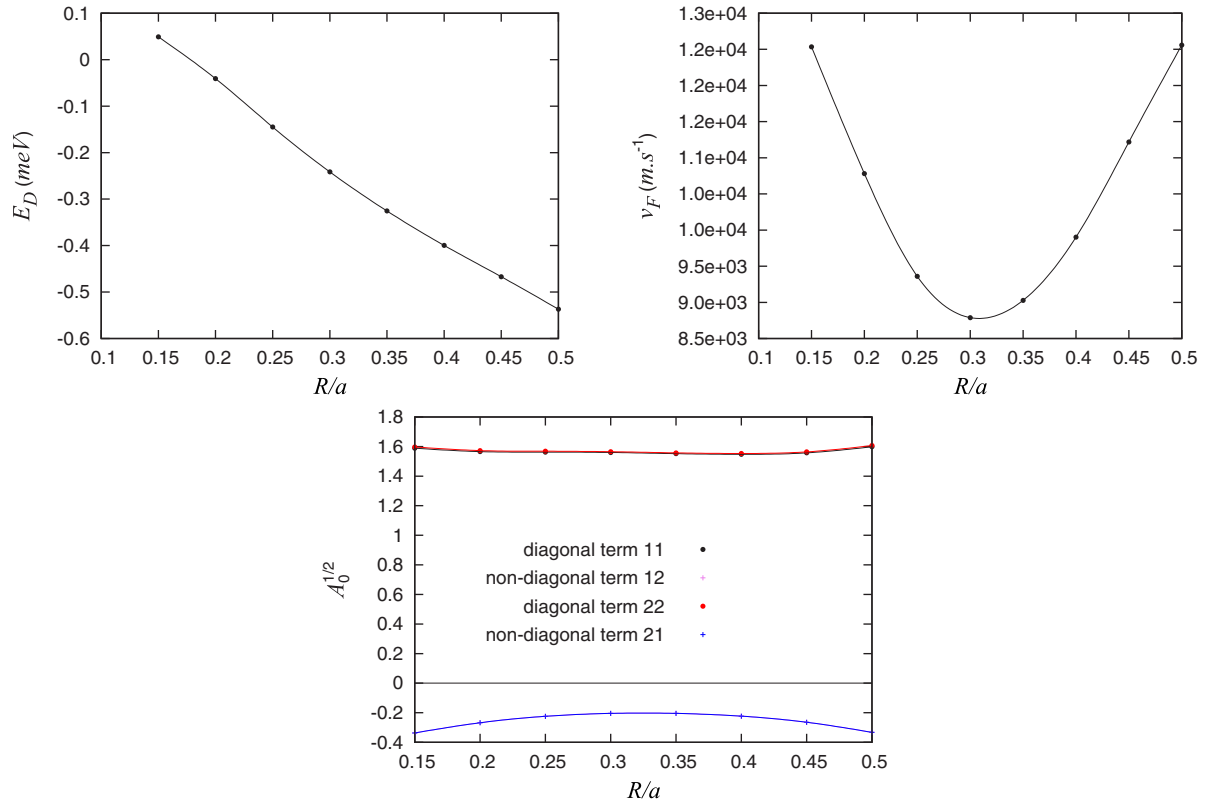
FIG. 8. (Color online) Dirac energy, Fermi velocity, and elements of the $\mathbf{A}_0^{1/2}$ matrix as a function of R/a obtained with the effective medium theory for the Dirac cone near the K point. In these simulations it was assumed that $V_0 = -0.8$ meV.

where $V_{\text{ef}}(E) = H_{\text{ef}}(\mathbf{k} = 0, E)$ and the inverse effective mass tensor is

$$\overline{\overline{m}}_{\text{ef}}^{-1}(E) = \frac{1}{\hbar^2} \begin{bmatrix} \frac{\partial^2 H_{\text{ef}}(\mathbf{k},E)}{\partial k_x^2}\Big|_{\mathbf{k}=0} & \frac{\partial^2 H_{\text{ef}}(\mathbf{k},E)}{\partial k_x \partial k_y}\Big|_{\mathbf{k}=0} \\ \frac{\partial^2 H_{\text{ef}}(\mathbf{k},E)}{\partial k_x \partial k_y}\Big|_{\mathbf{k}=0} & \frac{\partial^2 H_{\text{ef}}(\mathbf{k},E)}{\partial k_y^2}\Big|_{\mathbf{k}=0} \end{bmatrix}, \quad (54)$$
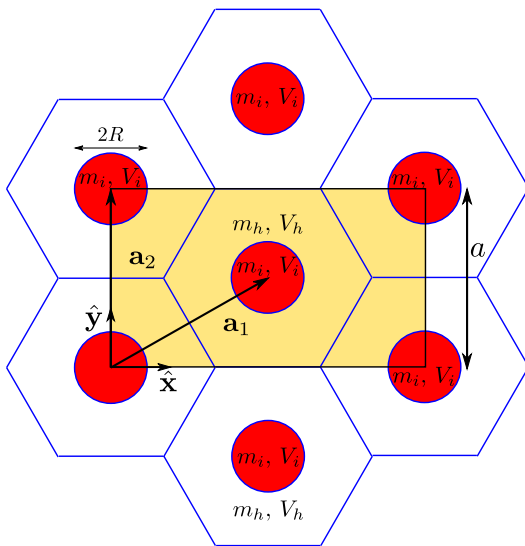

FIG. 9. (Color online) Hexagonal superlattice with primitive vectors $\mathbf{a}_1$ and $\mathbf{a}_2$. The potential and electron effective mass are V_h and m_h outside the disks, and V_i and m_i inside. The rectangular supercell used for the FDFD discretization is represented by the colored area.

with k_x and k_y the components of wave vector with respect to the x and y directions, respectively. Note that H_{ef} is an even function of $\mathbf{k}$. In particular, within the validity of Eq. (53) the energy-dependent effective Hamiltonian can be written in the space domain in the form

$$\hat{H}_{\text{ef}} = -\frac{\hbar^2}{2} \nabla \cdot \overline{\overline{m}}_{\text{ef}}^{-1}(E) \cdot \nabla + V_{\text{ef}}. \quad (55)$$

Based on an analogy with electromagnetic metamaterials, it was found in Ref. [22] that the effective mass tensor and the effective potential of the superlattice may be approximated by

$$m_{\text{ef}}(E) = m_h \frac{(1 - f_V)m_h + (1 + f_V)m_i}{(1 + f_V)m_h + (1 - f_V)m_i}, \quad (56)$$

$$V_{\text{ef}} = V_h(1 - f_V) + V_i f_V, \quad (57)$$

where f_V represents the volume fraction of the HgTe inclusions. In the next section, we compare these analytical formulas with the results obtained with the numerically calculated $H_{\text{ef}}(\mathbf{k}, E)$.

The dispersion of the electronic states of the superlattice can be found by solving the secular equation (13). In terms of the effective mass tensor and of the potential, it reduces to

$$\frac{\hbar^2}{2} \mathbf{k} \cdot \overline{\overline{m}}_{\text{ef}}^{-1}(E) \cdot \mathbf{k} = E - V_{\text{ef}}(E). \quad (58)$$

C. Numerical results

Using the formalism described in the previous section, we computed the effective parameters and the energy dispersion
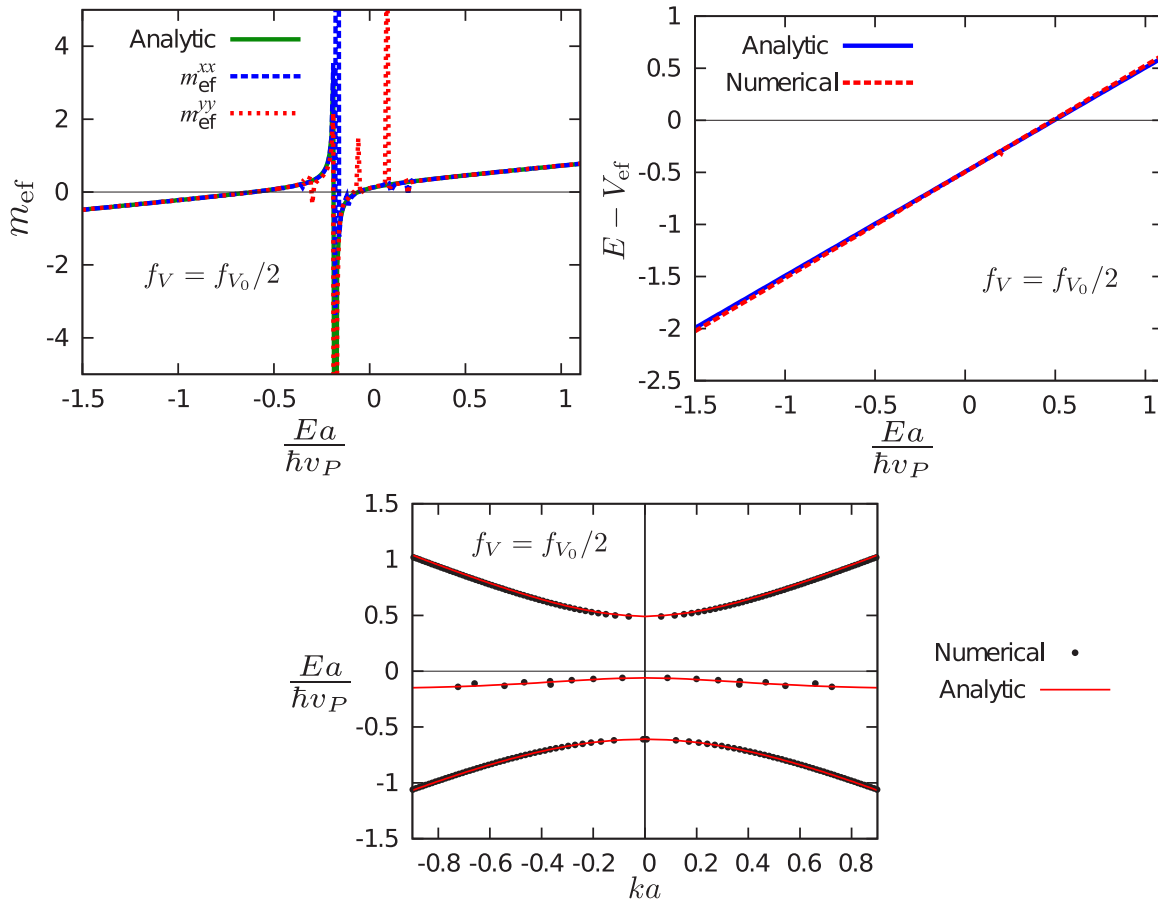
FIG. 10. (Color online) Effective parameters and electronic band structure near the Γ point for an HgCdTe superlattice with $f_V = f_{V_0}/2$. The solid lines represent the analytical results, whereas the discrete symbols/dashed lines are obtained from the numerically calculated effective Hamiltonian.

diagrams for different $Hg_{0.75}Cd_{0.25}Te$-HgTe superlattices with a lattice constant $a = 12a_s$, where $a_s = 0.65$ nm is the atomic lattice constant of the semiconductors. In our previous work, it was predicted that for a critical volume fraction of the inclusions,

$$f_{V_0} = \frac{E_{v,h} + E_{v,i} - 2V_h}{E_{v,h} - E_{v,i} - 2(V_h - V_i)}, \qquad (59)$$

the superlattice is characterized by a zero band gap at the energy level $E = V_{ef}$, where V_{ef} is given by Eq. (57). For the considered superlattice, $f_{V_0} = 0.247$.

Figures 10, 11, and 12 represent the numerically calculated effective parameters $E - V_{ef}$ and $\overline{\overline{m}}_{ef}$ and the energy dispersion for the volume fractions $f_{V_0}/2$, f_{V_0}, and $2f_{V_0}$, respectively. The out-of-diagonal components of the effective mass tensor are zero, and hence only the diagonal components are represented in the figures. The effective medium results correspond to the discrete symbols/dashed lines and are superimposed on the results (solid lines) predicted by the analytical formulas (56) and (57). In the simulations, we fixed the energy scale so that when $f_V = f_{V_0}$ the tip of the Dirac cone is associated with the energy level $E = 0$. This corresponds to choosing $E_{v,i}$ such that $(E_{v,h} + E_{v,i})V_i - 2E_{v,i}V_h = 0$ [22]. As seen, there is an excellent agreement between the analytic and effective medium results. Moreover, in Ref. [22], it was shown

that the analytical formulas compare very well with exact electronic band structure calculations based on the plane-wave method. This demonstrates that the single-component effective Hamiltonian describes correctly the propagation of electron waves in the HgCdTe superlattice, and thus that the electrons do not have a pseudospin degree of freedom as in the modulated 2DEG studied in the first part of the paper. A comparison between Kane-like electrons in semiconductor heterostructures and Dirac-like electrons in graphene was also reported in Ref. [46].

It is important to mention that the effective medium parameters have several extra resonances, which are not predicted by the analytical formalism. These resonances are associated with hybridized heavy-hole states, and give rise to extra nearly flat bands in the electronic band diagrams (not shown). As already discussed in Ref. [22], this property is the semiconductor counterpart of "plasmons" in metallic photonic crystals [47,48]. The stationary states of the superlattice occur for the energy levels for which the effective parameters $E - V_{ef}$ and $\overline{\overline{m}}_{ef}$ have the same sign, in agreement with (58). The two effective parameters play a role similar to the permittivity and permeability in electromagnetics [21,42].

As found in Ref. [22], the electronic states of the superlattice associated with the energy $E = V_{ef}$ are electron-like (Γ_6 band), whereas the states associated with the energy for which $m_{ef} = 0$
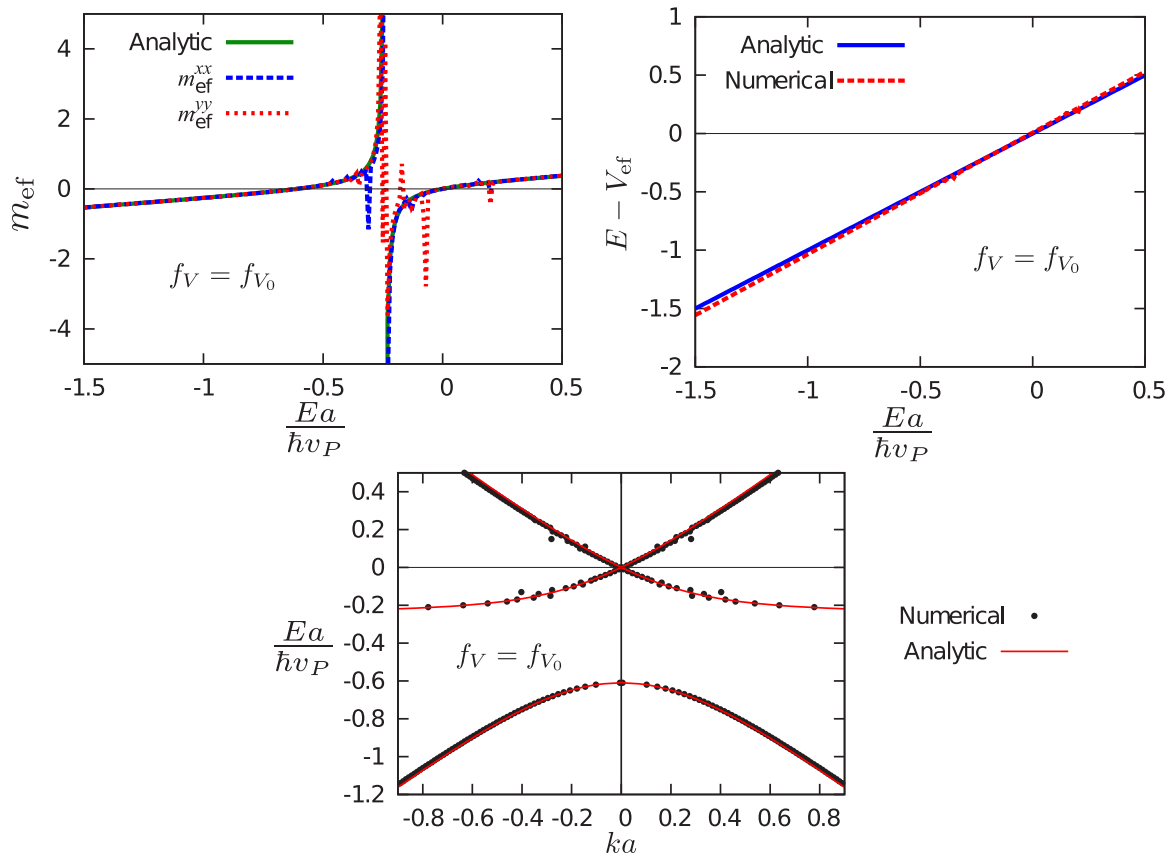
FIG. 11. (Color online) Similar to Fig. 10 but for $f_V = f_{V_0}$.

are light-hole-like (Γ_8 band). Thus the effective medium results of Figs. 10–12 confirm that for small values of f_V ($f_V < f_{V_0}$) the superlattice has a normal band structure similar to the host material, whereas for large values of f_V ($f_V > f_{V_0}$) the band structure is inverted similar to HgTe inclusions. The critical volume $f_V = f_{V_0}$ marks the topological transition from a normal to an inverted band structure, and is associated with a single valley Dirac cone at the Γ point. Because the electrons do not have a pseudospin, their time evolution is not described by a massless Dirac equation. Indeed, in the present case, the linear energy dispersion is not a consequence of a symmetry of the system, but rather due to the topological band structure transition. Related band structure transitions have been reported in HgCdTe quantum wells [39,40], and mark the point beyond which the transport associated with edge states becomes possible.

V. CONCLUSION

Using a first-principles effective medium approach, it was demonstrated that the electronic band structure of electron waves in a 2DEG modulated by an electrostatic potential with honeycomb symmetry is characterized by the massless 2D Dirac equation near the corners of the Brillouin zone, exactly as in graphene. Moreover, it was theoretically shown that the same formalism may also describe the time evolution of initial "macroscopic" electronic states, and the precise link

between the microscopic and effective medium frameworks was derived. In particular, our theory highlights the connection between the components of the pseudospinor and the values of the microscopic wave function in the two sublattices of the 2DEG. In addition, we characterized HgCdTe superlattices, and demonstrated that in this second platform the electrons can also have zero effective mass and linearly dispersing bands. However, different from the 2DEG artificial graphene, in this second system the electrons are achiral fermions and a pseudospinor description is not required. Moreover, the Dirac cone emerges at the Γ point and results from a topological band structure transition, rather than from the structural symmetry. Finally, we note that the ideas introduced in this paper can be readily extended to photonic systems, and may enable an effective medium description of electromagnetic waves in "photonic graphene" [13].

APPENDIX A: CALCULATION OF THE MICROSCOPIC WAVE FUNCTION WITH THE FDFD METHOD

In order to determine the solution $\psi(\mathbf{r}, \omega)$ of Eq. (8), we use the well-known FDFD method based on the Yee's
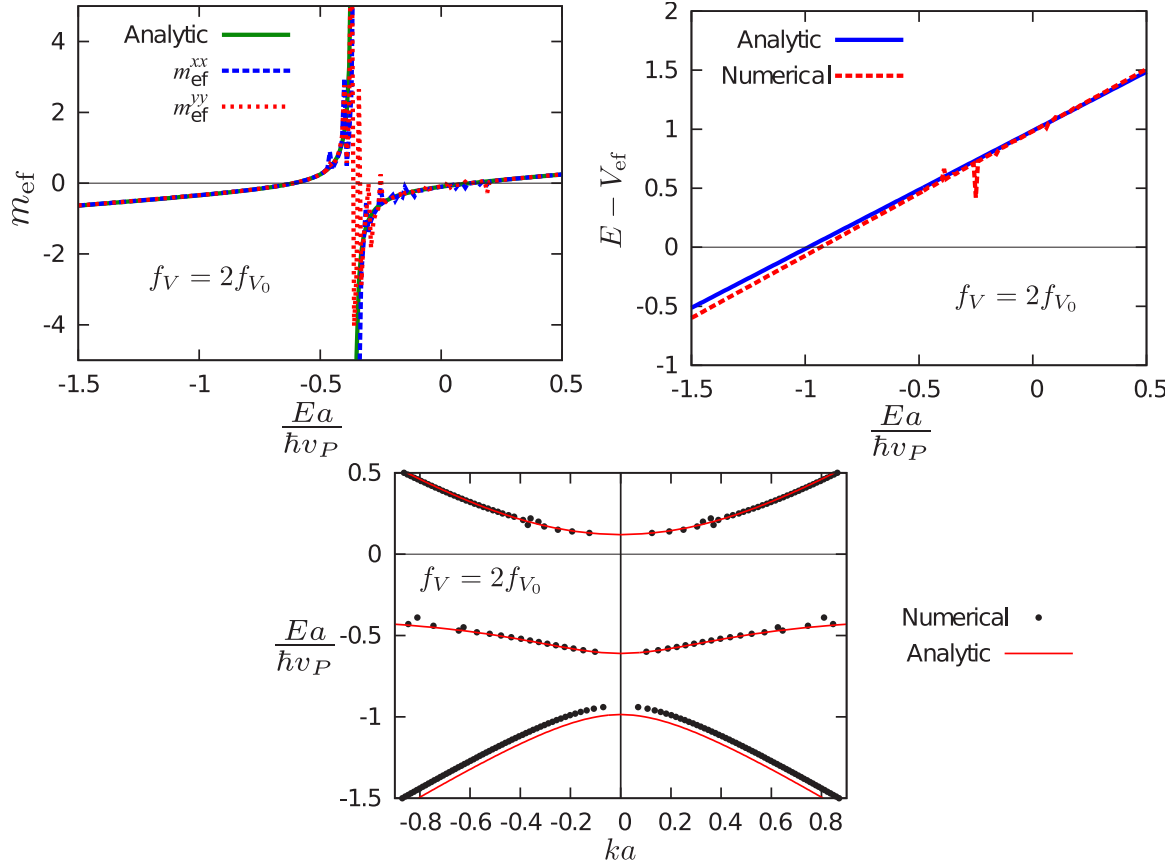
FIG. 12. (Color online) Similar to Fig. 10 but for $f_V = 2f_{V_0}$.

mesh [49]. This frequency domain method is well suited to model finite-sized structures with complex geometries. In this approach, the unit cell is divided into many rectangular subcells and the differential operators are replaced by finite difference operators on each node of the mesh.

1. Honeycomb lattice

Here, we describe the implementation of the FDFD method for the honeycomb lattice studied in Sec. II.

a. The unit cell

The primitive cell of the honeycomb lattice is not rectangular (see the region delimited by the dotted lines in Fig. 1), and consequently this cell is not adequate for the FDFD discretization of Eq. (8). Hence, to simplify the formulation of the FDFD problem, we use a rectangular supercell containing four elements and generated by the vectors $\mathbf{a}_1$ and $2\mathbf{a}_2 - \mathbf{a}_1$. This supercell is represented by the colored area in Fig. 1 (left). The coordinates of the primitive vectors in the Cartesian coordinate system are

$$\mathbf{a}_1 = a\sqrt{3}\hat{\mathbf{x}}, \tag{A1}$$

$$\mathbf{a}_2 = \frac{\sqrt{3}}{2}a\hat{\mathbf{x}} + \frac{3}{2}a\hat{\mathbf{y}}, \tag{A2}$$

where a is the nearest-neighbor distance.

The coordinates of the reciprocal lattice vectors $\mathbf{b}_1$ and $\mathbf{b}_2$ represented in Fig. 1 (right) are

$$\mathbf{b}_1 = \frac{2\pi}{a\sqrt{3}}\left(\hat{\mathbf{x}} - \frac{1}{\sqrt{3}}\hat{\mathbf{y}}\right), \tag{A3}$$

$$\mathbf{b}_2 = \frac{4\pi}{3a}\hat{\mathbf{y}}. \tag{A4}$$

b. FDFD discretization

For an initial macroscopic state $-i\hbar\psi_{t=0}(\mathbf{r}) = e^{i\mathbf{k}\cdot\mathbf{r}}$ (playing the role of a source), the problem to be solved [Eq. (8)] reduces to

$$\left[\frac{-\hbar^2}{2m_b}\left(\frac{\partial^2}{\partial x^2} + \frac{\partial^2}{\partial y^2}\right) + V(x,y) - E\right]\psi(\mathbf{r}) = e^{i\mathbf{k}\cdot\mathbf{r}}. \tag{A5}$$

As illustrated in Fig. 13, the supercell is discretized using a uniform grid, with N_x and N_y nodes along the x and y directions, respectively. The grid spacing along the x and y directions are $\Delta x = \frac{a\sqrt{3}}{N_x}$ and $\Delta y = \frac{3a}{N_y}$. The differential operators are discretized as in Refs. [50,51],

$$\frac{\partial^2\psi(i,j)}{\partial x^2} = \frac{\psi(i+1,j) - 2\psi(i,j) + \psi(i-1,j)}{(\Delta x)^2}, \tag{A6}$$

$$\frac{\partial^2\psi(i,j)}{\partial y^2} = \frac{\psi(i,j+1) - 2\psi(i,j) + \psi(i,j-1)}{(\Delta y)^2}. \tag{A7}$$
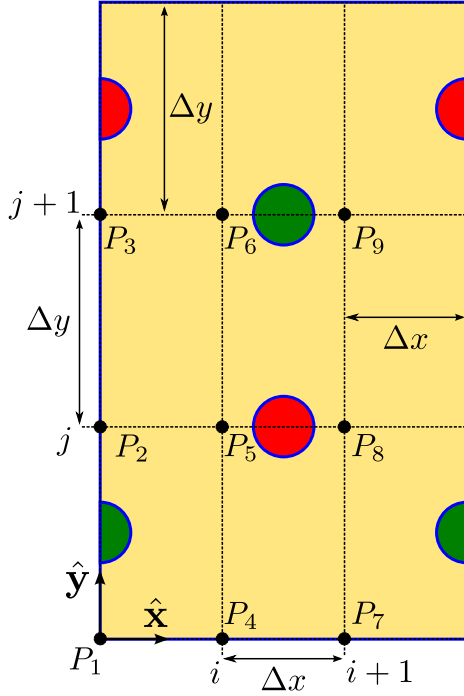
FIG. 13. (Color online) Geometry of the grid mesh for the FDFD discretization of the supercell in the particular case $N_x = N_y = 3$.

Hence Eq. (A5) reduces to

$$
\frac{-\hbar^2}{2m_b}\left(\frac{\psi(i+1,j) - 2\psi(i,j) + \psi(i-1,j)}{(\Delta x)^2}\right.
$$
$$
\left. + \frac{\psi(i,j+1) - 2\psi(i,j) + \psi(i,j-1)}{(\Delta y)^2}\right)
$$
$$
+ V(i,j) \cdot \psi(i,j) - E \cdot \psi(i,j) = e^{i\mathbf{k}\cdot\mathbf{r}(i,j)}, \quad \text{(A8)}
$$

where $\mathbf{r}(i,j)$ refers to the vector position at the node (i,j) of the grid (see Fig. 13). For the nodes located at the boundaries of the supercell, one or more adjacent node(s) may lie outside the grid. However, these nodes can be brought back inside the supercell using the Bloch-periodic boundary conditions:

$$
\psi(x + \|\mathbf{a}_1\|, y) = \psi(x + a\sqrt{3}, y) = \psi(x,y)e^{ik_x a\sqrt{3}}, \quad \text{(A9)}
$$

$$
\psi(x, y + \|2\mathbf{a}_2 - \mathbf{a}_1\|) = \psi(x, y + 3a) = \psi(x,y)e^{i3k_y a}, \quad \text{(A10)}
$$

where $\|\ \|$ refers to the norm of a vector, and k_x, k_y are the components of the wave vector along the x and y directions.

The system of equations (A8) is equivalent to a standard linear system with $N_x \times N_y$ equations and $N_x \times N_y$ unknowns [the $\psi(i,j)$]. This system can be solved with standard numerical methods, and its solution can then be used to compute the effective Hamiltonian as explained in Sec. II.

2. Hexagonal superlattice

The FDFD method implementation for the hexagonal superlattice studied in Sec. IV is very similar to what was described in the previous section. In this case, we used a

supercell generated by the primitive vectors $2\mathbf{a}_1 - \mathbf{a}_2$ and $\mathbf{a}_2$ (see the colored area in Fig. 9), with $\mathbf{a}_1 = \frac{\sqrt{3}}{2}a\hat{\mathbf{x}} + \frac{1}{2}a\hat{\mathbf{y}}$ and $\mathbf{a}_2 = a\hat{\mathbf{y}}$ and a the lattice constant. For an initial macroscopic state $-i\hbar\psi_{t=0}(\mathbf{r}) = e^{i\mathbf{k}\cdot\mathbf{r}}$, the equation to be solved is

$$
\frac{-\hbar^2}{2}\left[\frac{\partial}{\partial x}\left(\frac{1}{m(\mathbf{r})}\frac{\partial\psi(\mathbf{r})}{\partial x}\right) + \frac{\partial}{\partial y}\left(\frac{1}{m(\mathbf{r})}\frac{\partial\psi(\mathbf{r})}{\partial y}\right)\right]
$$
$$
+ V(\mathbf{r})\psi(\mathbf{r}) - E\psi(\mathbf{r}) = e^{i\mathbf{k}\cdot\mathbf{r}}. \quad \text{(A11)}
$$

The differential operators are discretized by using staggered subgrids for ψ, $\partial_x\psi$ and $\partial_y\psi$ similar to Yee's approach [49]. This gives

$$
\frac{\partial}{\partial x}\left(\frac{1}{m(i,j)}\frac{\partial\psi(i,j)}{\partial x}\right) = \frac{1}{(\Delta x)^2}\left(\frac{\psi(i+1,j) - \psi(i,j)}{m(i+\frac{1}{2},j)}\right.
$$
$$
\left. - \frac{\psi(i,j) - \psi(i-1,j)}{m(i-\frac{1}{2},j)}\right), \quad \text{(A12)}
$$

$$
\frac{\partial}{\partial y}\left(\frac{1}{m(i,j)}\frac{\partial\psi(i,j)}{\partial y}\right) = \frac{1}{(\Delta y)^2}\left(\frac{\psi(i,j+1) - \psi(i,j)}{m(i,j+\frac{1}{2})}\right.
$$
$$
\left. - \frac{\psi(i,j) - \psi(i,j-1)}{m(i,j-\frac{1}{2})}\right), \quad \text{(A13)}
$$

where the grid spacings along the x and y directions are $\Delta x = \frac{a\sqrt{3}}{N_x}$ and $\Delta y = \frac{a}{N_y}$. In this manner, the problem is reduced to a $N_x \times N_y$ linear system, analogous to the previous section.

APPENDIX B: PROBABILITY DENSITY FUNCTION IN THE EFFECTIVE MEDIUM APPROACH

In this Appendix, we demonstrate the relation (37) that links the microscopic and macroscopic probability densities. This result extends the findings of Refs. [29,31,52].

For convenience, we denote $\Phi_e = \{\Phi\}_{\text{av}}$ and introduce the inner product

$$
\langle\Phi_1|\Phi_2\rangle = \frac{1}{V_c}\int_\Omega \Phi_1^* \cdot \Phi_2\, d^N\mathbf{r}. \quad \text{(B1)}
$$

Moreover, it is easy to show that for a Bloch mode $g_\mathbf{k}$ with $\mathbf{k}$ in the Brillouin zone, we have the following property:

$$
\langle g_\mathbf{k}|g_\mathbf{k}\rangle = \{g_\mathbf{k}^* \cdot g_\mathbf{k}\}_{\text{av}}. \quad \text{(B2)}
$$

The starting point is to consider a family of solutions $\Phi = \Phi(\mathbf{r},E)$ of Eq. (20) parameterized by the energy E, and for initial conditions such that $f_1 = f_2 = f_0$. Thus $\Phi = \Phi(\mathbf{r},E)$ satisfies

$$
(\hat{H}_g - E) \cdot \Phi = \begin{pmatrix} \chi_1 & 0 \\ 0 & \chi_2 \end{pmatrix}\begin{pmatrix} 1 \\ 1 \end{pmatrix}f_0 e^{i\mathbf{k}\cdot\mathbf{r}}. \quad \text{(B3)}
$$

From Sec. III A and from the definition of the effective Hamiltonian, it is evident that

$$
(H_{g,\text{ef}}(\mathbf{k},E) - E) \cdot \Phi_e = \frac{1}{2}\begin{pmatrix} 1 \\ 1 \end{pmatrix}f_0 e^{i\mathbf{k}\cdot\mathbf{r}}. \quad \text{(B4)}
$$

Hence, by combining the two equations, it is possible to write

$$
(\hat{H}_g - E) \cdot \Phi = 2\begin{pmatrix} \chi_1 & 0 \\ 0 & \chi_2 \end{pmatrix} \cdot (H_{g,\text{ef}}(\mathbf{k},E) - E) \cdot \Phi_e. \quad \text{(B5)}
$$

Differentiating both sides with respect to E and taking the inner product of the resulting equation with Φ, we get

$$\left\langle \Phi \left| (\hat{H}_g - E) \cdot \frac{\partial \Phi}{\partial E} \right\rangle - \langle \Phi | \Phi \rangle \right.$$
$$= 2 \left\langle \Phi \left| \begin{pmatrix} \chi_1 & 0 \\ 0 & \chi_2 \end{pmatrix} \cdot [H_{g,\text{ef}}(\mathbf{k}, E) - E] \cdot \frac{\partial \Phi_e}{\partial E} \right\rangle \right.$$
$$- 2 \left\langle \Phi \left| \begin{pmatrix} \chi_1 & 0 \\ 0 & \chi_2 \end{pmatrix} \cdot \left(1 - \frac{\partial H_{g,\text{ef}}(\mathbf{k}, E)}{\partial E} \right) \cdot \Phi_e \right\rangle. \quad (B6)$$

Using the fact that $\begin{pmatrix} \chi_1 & 0 \\ 0 & \chi_2 \end{pmatrix} \cdot \Phi = \Phi$ and Eq. (22), it is found that

$$\left\langle \Phi \left| \begin{pmatrix} \chi_1 & 0 \\ 0 & \chi_2 \end{pmatrix} \cdot \left(1 - \frac{\partial H_{g,\text{ef}}(\mathbf{k}, E)}{\partial E} \right) \cdot \Phi_e \right\rangle \right.$$
$$= \left(\frac{1}{V_c} \int_\Omega \Phi^* e^{i\mathbf{k} \cdot \mathbf{r}} \, d^N \mathbf{r} \right) \cdot \left(1 - \frac{\partial H_{g,\text{ef}}(\mathbf{k}, E)}{\partial E} \right) \cdot \Phi_{\text{av}}$$
$$= \Phi_e^* \cdot \left(1 - \frac{\partial H_{g,\text{ef}}(\mathbf{k}, E)}{\partial E} \right) \cdot \Phi_e. \quad (B7)$$

Based on similar arguments, it is possible to verify that

$$\left\langle \Phi \left| \begin{pmatrix} \chi_1 & 0 \\ 0 & \chi_2 \end{pmatrix} \cdot [H_{g,\text{ef}}(\mathbf{k}, E) - E] \cdot \frac{\partial \Phi_e}{\partial E} \right\rangle \right.$$
$$= \Phi_e^* \cdot [H_{g,\text{ef}}(\mathbf{k}, E) - E] \cdot \frac{\partial \Phi_e}{\partial E}. \quad (B8)$$

On the other hand, because $\hat{H}_g$ is Hermitian (thus $H_{g,\text{ef}}$ is also an Hermitian matrix) and from Eq. (B5), it follows that

$$\left\langle \Phi \left| (\hat{H}_g - E) \frac{\partial \Phi}{\partial E} \right\rangle \right.$$
$$= \left\langle 2 \begin{pmatrix} \chi_1 & 0 \\ 0 & \chi_2 \end{pmatrix} \cdot \left(H_{g,\text{ef}}(\mathbf{k}, E) - E \right) \cdot \Phi_e \left| \frac{\partial \Phi}{\partial E} \right\rangle \right.$$

$$= 2 \left\langle \Phi_e \left| (H_{g,\text{ef}}(\mathbf{k}, E) - E) \cdot \begin{pmatrix} \chi_1 & 0 \\ 0 & \chi_2 \end{pmatrix} \cdot \frac{\partial \Phi}{\partial E} \right\rangle \right.$$
$$= 2 \Phi_e^* \cdot [H_{g,\text{ef}}(\mathbf{k}, E) - E] \cdot \frac{\partial \Phi_e}{\partial E}. \quad (B9)$$

Then by substitution of the previous results into (B6), we conclude that

$$\langle \Phi | \Phi \rangle = 2 \Phi_e^* \cdot \left(1 - \frac{\partial H_{g,\text{ef}}(\mathbf{k}, E)}{\partial E} \right) \cdot \Phi_e. \quad (B10)$$

This result and Eq. (B2) yield (37), as we wanted to prove. Note that because f_0 in Eq. (B4) is an arbitrary function of the energy, the derived result applies to any solution of (B4), and in particular to the electronic stationary states $[f_0(E) = 0]$.

APPENDIX C: THE MATRICES $\tilde{\mathbf{A}}_1$ AND $\tilde{\mathbf{A}}_2$

To illustrate the accuracy of the identities in Eq. (44), we consider the particular case wherein the structural parameters of the 2DEG satisfy $V_0 = -0.8$ meV and $R/a = 0.35$, as in Fig. 2. The numerically computed matrices are such that (showing three significant figures)

$$\frac{1}{\hbar v_F \cos \phi} \text{Re}(\tilde{\mathbf{A}}_1) = \begin{pmatrix} -5.39 \times 10^{-3} & 0.999 \\ 0.999 & 8.97 \times 10^{-3} \end{pmatrix}, \quad (C1)$$

$$\frac{1}{\hbar v_F \sin \phi} \text{Re}(\tilde{\mathbf{A}}_2) = \begin{pmatrix} 6.62 \times 10^{-3} & 1.00 \\ 1.00 & -6.03 \times 10^{-3} \end{pmatrix}, \quad (C2)$$

$$\frac{-1}{\hbar v_F \sin \phi} \text{Im}(\tilde{\mathbf{A}}_1) = \begin{pmatrix} -7.84 \times 10^{-11} & -0.999 \\ 0.999 & -8.35 \times 10^{-10} \end{pmatrix}, \quad (C3)$$

$$\frac{1}{\hbar v_F \cos \phi} \text{Im}(\tilde{\mathbf{A}}_2) = \begin{pmatrix} -2.26 \times 10^{-11} & -1.00 \\ 1.00 & 2.05 \times 10^{-9} \end{pmatrix}, \quad (C4)$$

with $\phi = 60°$ and $v_F = 9.03 \times 10^3$ m s^{-1}. These results demonstrate that Eq. (44) is very accurate.

[1] K. S. Novoselov, A. K. Geim, S. V. Morozov, D. Jiang, Y. Zhang, S. V. Dubonos, I. V. Grigorieva, and A. A. Firsov, Science **306**, 666 (2004).

[2] A. H. Castro Neto, F. Guinea, N. M. R. Peres, K. S. Novoselov, and A. K. Geim, Rev. Mod. Phys. **81**, 109 (2009).

[3] S. D. Sarma, S. Adam, E. H. Hwang, and E. Rossi, Rev. Mod. Phys. **83**, 407 (2011).

[4] A. Vakil and N. Engheta, Science **332**, 1291 (2011).

[5] F. H. L. Koppens, D. E. Chang, and F. J. G. de Abajo, Nano Lett. **11**, 3370 (2011).

[6] F. J. G. de Abajo, ACS Photon. **1**, 135 (2014).

[7] A. N. Grigorenko, M. Polini, and K. S. Novoselov, Nat. Photon. **6**, 749 (2012).

[8] S. A. Mikhailov and K. Ziegler, J. Phys.: Condens. Matter **20**, 384204 (2008).

[9] S.-L. Zhu, B. Wang, and L.-M. Duan, Phys. Rev. Lett. **98**, 260402 (2007).

[10] C. Wu, D. Bergman, L. Balents, and S. Das Sarma, Phys. Rev. Lett. **99**, 070401 (2007).

[11] C. Wu and S. Das Sarma, Phys. Rev. B **77**, 235107 (2008).

[12] B. Wunsch, F. Guinea, and F. Sols, New J. Phys. **10**, 103027 (2008).

[13] O. Peleg, G. Bartal, B. Freedman, O. Manela, M. Segev, and D. N. Christodoulides, Phys. Rev. Lett. **98**, 103901 (2007).

[14] M. Polini, F. Guinea, M. Lewenstein, H. C. Manoharan, and V. Pellegrini, Nat. Nanotechnol. **8**, 625 (2013).

[15] A. Singha, M. Gibertini, B. Karmakar, S. Yuan, M. Polini, G. Vignale, M. I. Katsnelson, A. Pinczuk, L. N. Pfeiffer, K. W. West, and V. Pellegrini, Science **332**, 1176 (2011).

[16] C.-H. Park and S. G. Louie, Nano Lett. **9**, 1793 (2009).

[17] M. Gibertini, A. Singha, V. Pellegrini, M. Polini, G. Vignale, A. Pinczuk, L. N. Pfeiffer, and K. W. West, Phys. Rev. B **79**, 241406 (2009).

[18] M. G. Silveirinha and N. Engheta, Phys. Rev. B **85**, 195413 (2012).

[19] L. Esaki and R. Tsu, IBM J. Res. Dev. **14**, 61 (1970).

[20] M. G. Silveirinha and N. Engheta, Phys. Rev. B **86**, 161104(R) (2012).

[21] M. G. Silveirinha and N. Engheta, Phys. Rev. B **86**, 245302 (2012).

[22] M. G. Silveirinha and N. Engheta, Phys. Rev. B **89**, 085205 (2014).

[23] G. Bastard, *Wave Mechanics Applied to Semiconductor Heterostructures* (Wiley, New York, 1988).

[24] L. C. L. Y. Voon and M. Willatzen, *The k p Method: Electronic Properties of Semiconductors* (Springer, Berlin, 2009).

[25] M. G. Burt, J. Phys.: Condens. Matter **4**, 6651 (1992).

[26] M. G. Burt, J. Phys.: Condens. Matter **11**, R53 (1999).

[27] B. A. Foreman, Phys. Rev. B **48**, 4964 (1993).

[28] M. F. Pereira Jr., I. Galbraith, S. W. Koch, and G. Duggan, Phys. Rev. B **42**, 7084 (1990).

[29] M. G. Silveirinha, Phys. Rev. B **80**, 235120 (2009).

[30] M. G. Silveirinha and N. Engheta, Phys. Rev. Lett. **110**, 213902 (2013).

[31] D. E. Fernandes, N. Engheta, and M. G. Silveirinha, Phys. Rev. B **90**, 041406(R) (2014).

[32] M. G. Silveirinha, Phys. Rev. B **75**, 115104 (2007).

[33] M. G. Silveirinha, Phys. Rev. B **83**, 165104 (2011).

[34] A. Alu, Phys. Rev. B **84**, 075153 (2011).

[35] C. Fietz and G. Shvets, Physica B **405**, 2930 (2010).

[36] N. W. Ashcroft and N. D. Mermin, *Solid State Physics* (Saunders College, Philadelphia, 1976).

[37] J. D. Joannopoulos, S. G. Johnson, J. N. Winn, and R. D. Meade, *Photonic Crystals: Molding the Flow of Light*, 2nd ed. (Princeton University Press, Princeton, New Jersey, 2008).

[38] L. D. Landau and E. M. Lifshitz, *Electrodynamics of Continuous Media, Course of Theoretical Physics* (Elsevier Butterworth-Heinemann, Oxford, 2004), Vol. 8.

[39] B. A. Bernevig, T. L. Hughes, and S.-C. Zhang, Science **314**, 1757 (2006).

[40] M. Konig, S. Wiedmann, C. Brune, A. Roth, H. Buhmann, L. W. Molenkamp, X.-L. Qi, and S.-C. Zhang, Science **318**, 766 (2007).

[41] S. L. Chuang, *Physics of Optoelectronic Devices* (John Wiley & Sons, Hoboken, 1995).

[42] L. Jelinek, J. D. Baena, J. Voves, and R. Marques, New J. Phys. **13**, 083011 (2011).

[43] A. Rogalski, Rep. Prog. Phys. **68**, 2267 (2005).

[44] G. L. Hansen, J. L. Schmit, and T. N. Casselman, J. Appl. Phys. **53**, 7099 (1982).

[45] P. Lawaetz, Phys. Rev. B **4**, 3460 (1971).

[46] D. Dragoman, J. Appl. Phys. **108**, 094302 (2010).

[47] A. R. McGurn and A. A. Maradudin, Phys. Rev. B **48**, 17576 (1993).

[48] J. T. Costa and M. G. Silveirinha, Phys. Rev. B **84**, 155131 (2011).

[49] K. Yee, IEEE Trans. Antennas Propagat. **14**, 302 (1966).

[50] K. Yasumoto, *Electromagnetic Theory and Applications for Photonic Crystals* (Taylor and Francis, New York, 2006).

[51] J. T. Costa, M. G. Silveirinha, and S. I. Maslovski, Phys. Rev. B **80**, 235124 (2009).

[52] J. T. Costa, M. G. Silveirinha, and A. Alu, Phys. Rev. B **83**, 165120 (2011).